Title

Syntheses and properties of phosphine-substituted ruthenium(ii) polypyridine complexes with nitrogen oxides

Journal

Dalton Transactions, 44(39)

ISSN

1477-9226

Authors

Nakamura, Go
Kondo, Mio
Crisalli, Meredith
et al.

Publication Date

2015-10-21

DOI

10.1039/c5dt02994e

Peer reviewed

Dalton Transactions

PAPER

View Article Online
View Journal | View Issue

Cite this: *Dalton Trans.*, 2015, **44**, 17189

Syntheses and properties of phosphine-substituted ruthenium(II) polypyridine complexes with nitrogen oxides†

Go Nakamura,[a,b] Mio Kondo,[a,b,c,d] Meredith Crisalli,[e] Sze Koon Lee,[a] Akane Shibata,[a] Peter C. Ford[e] and Shigeyuki Masaoka*[a,b,d]

Received 4th August 2015,
Accepted 27th August 2015

DOI: 10.1039/c5dt02994e

www.rsc.org/dalton

Four novel phosphine-substituted ruthenium(II) polypyridine complexes with nitrogen oxides—*trans*-(P,NO_2)-[Ru(trpy)(Pqn)(NO_2)]PF_6 (***trans*-NO$_2$**), *cis*(P,NO_2)-[Ru(trpy)(Pqn)(NO_2)]PF_6 (***cis*-NO$_2$**), [Ru(trpy)(dppbz)(NO_2)]PF_6 (**PP-NO$_2$**), and *cis*(P,NO)-[Ru(trpy)(Pqn)(NO)]$(PF_6)_3$ (***cis*-NO**)—were synthesised (trpy = 2,2′:6′,2″-terpyridine, Pqn = 8-(diphenylphosphanyl)quinoline, and dppbz = 1,2-bis(diphenylphosphanyl)benzene). The influence of the number and position of the phosphine group(s) on the electronic structure of these complexes was investigated using single-crystal X-ray structural analysis, UV-vis absorption spectroscopy, and electrochemical measurements. The substitution lability of the nitrogen oxide ligand of each complex is discussed in comparison with that of the corresponding acetonitrile complexes.

Introduction

Ruthenium(II) polypyridine complexes are widely studied materials because of their contributions to fundamental coordination chemistry, including electrochemistry, photochemistry, and photophysics,[1] and their potential applications in energy conversion,[2] luminescent sensors,[3] electroluminescence displays,[4] and biotechnology.[5] Of particular interest are the Ru(II) complexes $[Ru(TL)(BL)(L)]^{n+}$ (TL = tridentate polypyridine ligand, BL = bidentate polypyridine ligand, and L = monodentate labile ligand) given their catalytic activity for various reactions, such as oxidation,[6,7] reduction,[8–11] and photo-induced reactions.[12]

Phosphine-containing ruthenium(II) complexes are also attractive for potential applications in energy conversion systems[13] and catalysis[14–17] owing to the σ-donating and π-accepting abilities of the phosphine ligands. Thus, it should be possible to develop ruthenium complexes that have novel and tunable properties and reactivity by designing mixed polypyridyl/phosphine complexes. There have been several reports on the syntheses of ruthenium(II) polypyridine complexes containing monodentate phosphine ligands[16,18,19] and their catalytic activities.[19d,20] However, ruthenium(II) polypyridine complexes of the type $[Ru(TL)(BL)(L)]^{n+}$ bearing bidentate ligands with P and N donors have not been investigated.

In our previous report,[21] we synthesised and structurally characterised for the first time a series of phosphine-containing ruthenium(II) polypyridine complexes of the type $[Ru(TL)(BL)(L)]^{n+}$, with L = acetonitrile, TL = 2,2′:6′,2″-terpyridine (trpy), and BL = 8-(diphenylphosphanyl)quinoline (Pqn) or 1,2-bis(diphenylphosphanyl)benzene (dppbz) (Scheme 1). The influence of the number and position of phosphine donors on the structures and electronic properties was characterised, and unique isomerisation behaviours of these complexes were observed. The coordinating phosphorus ligands played a crucial role in these isomerisation reactions, and the results encouraged us to investigate in more detail the influence of the P atom on the physical properties of Ru-based metal complexes.

In this study, we investigated the reaction of phosphine-containing ruthenium complexes with the nitrogen oxides, NO and NO_2^-, because of their biological roles as signalling molecules[22] and reservoirs,[23] in addition to the fundamental interest in their coordination chemistry. Here, we show the syntheses, structural characterisation, and electrochemical and spectroscopic properties of a series of ruthenium(II)

[a]*Institute for Molecular Science (IMS), 5-1 Higashiyama, Myodaiji, Okazaki, Aichi 444-8787, Japan. E-mail: masaoka@ims.ac.jp; Fax: +81-564-59-5589*
[b]*Department of Structural Molecular Science, School of Physical Sciences, SOKENDAI (The Graduate University for Advanced Studies), Shonan Village, Hayama-cho, Kanagawa 240-0193, Japan*
[c]*ACT-C, Japan Science and Technology Agency (JST), 4-1-8 Honcho, Kawaguchi, Saitama 332-0012, Japan*
[d]*Research Center of Integrative Molecular Systems (CIMoS), Institute for Molecular Science, 38 Nishigo-naka, Myodaiji, Okazaki, Aichi 444-8585, Japan*
[e]*Department of Chemistry and Biochemistry, University of California at Santa Barbara, Santa Barbara, California 93106-9510, USA*
† Electronic supplementary information (ESI) available. CCDC 1040452–1040454. For ESI and crystallographic data in CIF or other electronic format see DOI: 10.1039/c5dt02994e

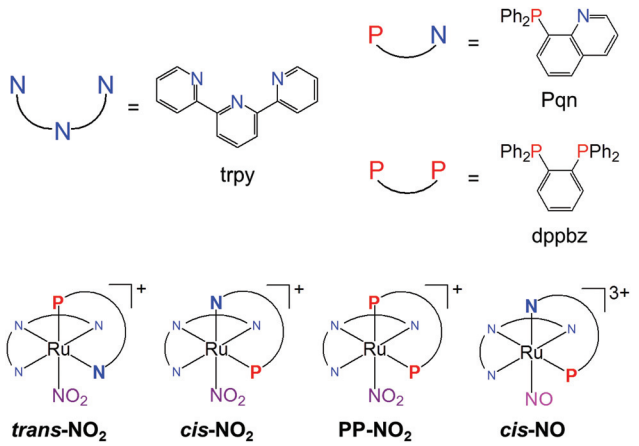

Scheme 1 Structures of a tridentate ligand (trpy), bidentate ligands (Pqn and dppbz), and metal complexes (***trans*-NO$_2$**, ***cis*-NO$_2$**, **PP-NO$_2$**, and ***cis*-NO**) used in this study.

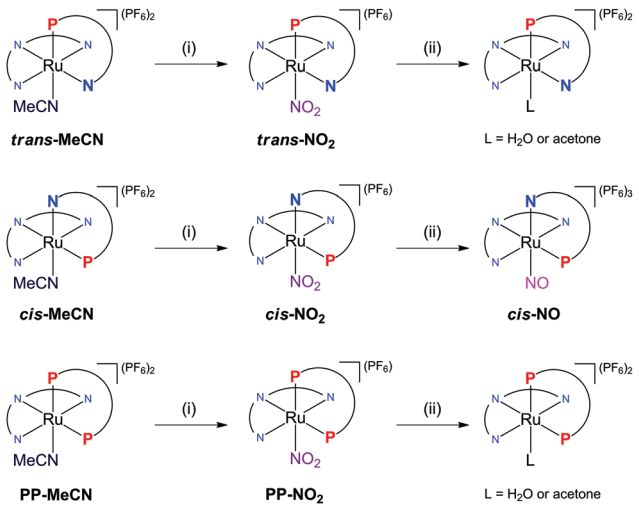

Scheme 2 Syntheses of ***trans*-NO$_2$**, ***cis*-NO$_2$**, **PP-NO$_2$**, and ***cis*-NO**. (i) $NaNO_2$ in a 1 : 1 mixture of ethanol : water at 100 °C. (ii) HPF_6 in acetone at 0 °C.

polypyridine complexes containing Pqn or dppbz with nitric oxides. Three novel nitrito-κ*N* complexes—*trans*(P,NO_2)- and *cis*(P,NO_2)-[Ru(trpy)(Pqn)(NO_2)]PF_6 (***trans*-NO$_2$** and ***cis*-NO$_2$**), and [Ru(trpy)(dppbz)(NO_2)]PF_6 (**PP-NO$_2$**)—were successfully synthesised. Described here are the single-crystal X-ray structural determinations, UV-vis absorption spectra, and electrochemical measurements for these complexes, and the preparation of the nitrosyl complex *cis*(P,NO)-[Ru(trpy)(Pqn)(NO)]$(PF_6)_3$ (***cis*-NO**) from ***cis*-NO$_2$** and its properties are examined. The present study allows us to probe systematically the chemical and structural properties of phosphine-containing ruthenium complexes with nitrogen oxides by the use of the geometric isomers of the Pqn complex. Additionally, other reactivity properties and comparisons with those of the corresponding acetonitrile complexes are presented.

Results and discussion

Syntheses and characterisation

The synthetic procedures to obtain ***trans*-NO$_2$**, ***cis*-NO$_2$**, and **PP-NO$_2$** are shown in Scheme 2. The precursors, ***trans*-MeCN**, ***cis*-MeCN**, and **PP-MeCN**, were synthesised according to the method that we previously reported.[21] The reaction of the respective acetonitrile complexes with excess $NaNO_2$ in a 1 : 1 mixture of ethanol : water at 100 °C gave the corresponding nitrito-κ*N* complexes (***trans*-NO$_2$**, ***cis*-NO$_2$**, and **PP-NO$_2$**).[24,26b] The resulting products were characterised by ^{1}H NMR and $^{31}P\{^1H\}$ NMR spectroscopy and elemental analysis.

The $^{31}P\{^1H\}$ NMR spectra of ***trans*-NO$_2$** and ***cis*-NO$_2$** in CD_3CN displayed singlets at δ 53.10 and 54.06, respectively, showing upfield shifts ($\Delta\delta$ = 5.70 and 1.90) compared to the spectra of the corresponding acetonitrile complexes, ***trans*-MeCN** and ***cis*-MeCN** (δ 58.80 and 55.96). The $^{31}P\{^1H\}$ NMR spectrum of **PP-NO$_2$** in CD_3CN afforded two doublets at δ 62.65 and 68.59 with coupling constants of 14.2 Hz, again showing upfield shifts ($\Delta\delta$ = 5.85 and 1.18, respectively) compared with the spectrum of **PP-MeCN** (68.57 and 69.77, $^2J_{P-P}$ = 20.2 Hz).

Conversions of the nitrito-κ*N* complexes to the corresponding ruthenium nitrosyls were attempted by adding an excess of HPF_6 to acetone solutions of the nitrito-κ*N* species at 0 °C. The preparations of ***trans*-NO** and **PP-NO** from ***trans*-NO$_2$** and **PP-NO$_2$**, respectively, were not successful because of the instability of the nitrosyl complex or of a reaction intermediate under acidic conditions (for details, see Fig. S1 and S2 in the ESI†). However, ***cis*-NO** was isolated in 85% yield and was characterised by ^{1}H and $^{31}P\{^1H\}$ NMR spectroscopy and elemental analysis. The $^{31}P\{^1H\}$ NMR spectrum of ***cis*-NO** in acetone-d_6 gave a singlet at δ 54.23. ***cis*-NO** immediately converted to a solvent-coordinated complex in acetonitrile (Fig. S3 in the ESI†) but was meta-stable in weaker-coordinating solvents, such as acetone, γ-butyrolactone and ethylene glycol (Fig. S4 in the ESI†). The difference in the stability of these nitrosyl complexes will be discussed in the "Substitution lability of nitrogen oxide" section.

Crystal structures

Single crystals of ***trans*-NO$_2$** and **PP-NO$_2$** suitable for structural determination were obtained by recrystallisation from diethyl ether/methanol/acetonitrile. Single crystals of the *cis*-nitrito-κ*N* complex were obtained as the BPh_4^- salt, *cis*(P,NO_2)-[Ru(trpy)(Pqn)(NO_2)]BPh_4 (***cis*-NO$_2$′**), by adding an excess of $NaBPh_4$, instead of NH_4PF_6, after the reaction. The molecular structures of ***trans*-NO$_2$**, ***cis*-NO$_2$′**, and **PP-NO$_2$** determined by single-crystal X-ray crystallography and the summary of crystallographic data are shown in Fig. 1 and Table 1, respectively. The asymmetric unit of the monoclinic $P2_1/n$ crystal of ***trans*-NO$_2$** contained one cationic ruthenium complex, one PF_6 anion, and one acetonitrile molecule. The ***cis*-NO$_2$′** crystallised with

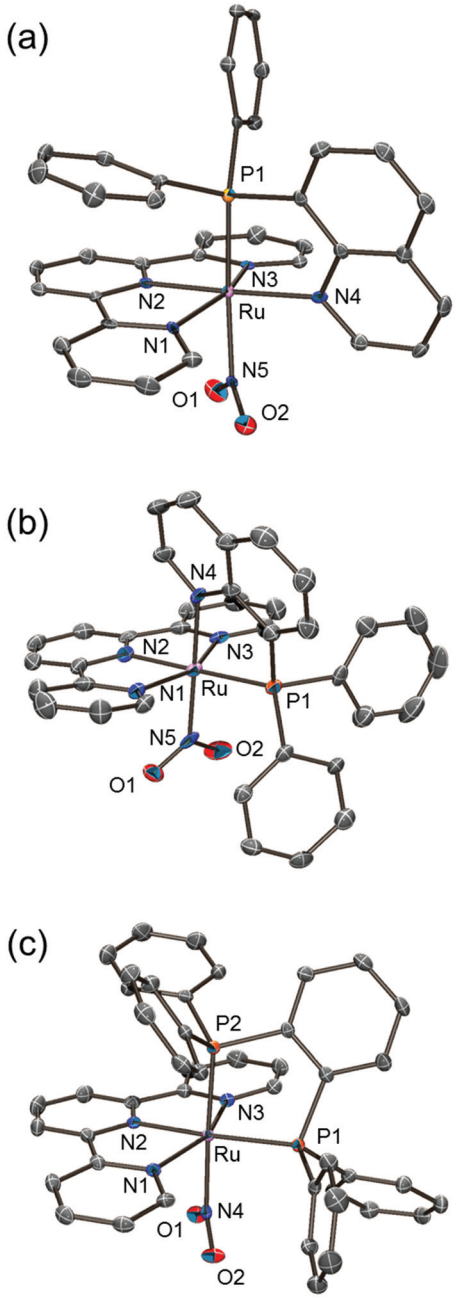

Fig. 1 ORTEP drawings (50% probability level) of cationic complexes in (a) ***trans*-NO$_2$**, (b) ***cis*-NO$_2$′**, and (c) **PP-NO$_2$**. Hydrogen atoms are omitted for clarity.

two crystallographically independent ruthenium complexes, two BPh_4^- anions, and one acetonitrile molecule as the crystal solvent in the asymmetric unit of the triclinic *P*1 space group. The asymmetric unit of the monoclinic $P2_1/c$ crystal of **PP-NO$_2$** contained one cationic ruthenium complex, one PF_6 anion, and two methanol molecules. For each complex, the ratio of ruthenium to counter anion indicated that the oxidation state of the ruthenium centre was +2. The coordination geometry of each Ru atom was that of a distorted octahedron composed of a meridionally coordinated terpyridine ligand, a bidentate ligand, and a nitrito ligand.

The bond distances between the ruthenium and nitrogen atoms of the nitrito ligand of ***trans*-NO$_2$** and **PP-NO$_2$** were 2.146(4) (Ru1–N5) and 2.124(2) Å (Ru1–N4), respectively (Fig. 2), and were longer than those found in [Ru(trpy)(bpm)(NO_2)]PF_6 (2.034(5) Å, bpm = 2,2′-bipyrimidine).[25] By contrast, the Ru–N(NO_2) distances in ***cis*-NO$_2$′** (2.0362(18) and 2.0290 (18) Å for Ru1–N5 and Ru2–N10, respectively, Fig. 2) were similar to those of [Ru(trpy)(bpm)(NO_2)]PF_6 (2.034(5) Å). These results indicated a stronger *trans* influence of the phosphorus atom of Pqn or dppbz compared with that of the nitrogen atom of bpm or bpy. This tendency was also observed in ***trans*-MeCN**, ***cis*-MeCN**, and **PP-MeCN** in our previous study.[21]

UV-vis absorption spectra

Fig. 3 shows the UV-Vis absorption spectra of the nitrito-κ*N* complexes, ***trans*-NO$_2$**, ***cis*-NO$_2$**, and **PP-NO$_2$**, in acetonitrile solution. The spectral data for these complexes and related compounds are listed in Table 2. All complexes displayed intense absorption bands in the UV region that were assigned to ligand-based π–π* transitions. Additionally, a moderately intense band was observed in the visible region for each complex. TD-DFT calculations that were performed at the B3LYP/LANL2DZ and B3LYP/SDD level of theory indicated that the visible region band could be assigned to metal-to-ligand charge transfer (MLCT) transitions from the dπ orbitals of ruthenium to the π* orbitals of trpy and Pqn or dppbz (for details, see Table S1 and Fig. S5–9 in the ESI†). The molar absorption coefficient of **PP-NO$_2$** was nearly half of those of ***trans*-NO$_2$** and ***cis*-NO$_2$**. The absorption maximum (λ_{max}) of the MLCT transition of ***trans*-NO$_2$**, ***cis*-NO$_2$**, and **PP-NO$_2$** was 443, 431, and 402 nm, respectively, and was blue-shifted compared with that of [Ru(trpy)(bpm)(NO_2)]PF_6,[25] suggesting the stabilisation of the dπ orbitals of the ruthenium centre upon introduction of the phosphine donors. Note that the MLCT band of ***cis*-NO$_2$** was more blue-shifted than that of ***trans*-NO$_2$** despite their isomeric relationship. A similar pattern was noted for the acetonitrile complexes, ***trans*-MeCN**, ***cis*-MeCN**, and **PP-MeCN**.[21]

The UV-vis absorption spectra of the *cis*-isomers with different ligands L, *cis*(P,L)-$[Ru(trpy)(Pqn)(L)]^{n+}$ (L = Cl^-, NO_2^-, MeCN, and NO^+), in ethylene glycol solution are shown in Fig. 4. These complexes each exhibited ligand-based π–π* transitions in the UV region and MLCT transitions in the visible region. The MLCT transition of ***cis*-NO** was observed at λ_{max} = 383 nm and is comparable to similar Ru–NO complexes (Table 3). For the different Ls, the lowest energy MLCT bands of the *cis*-isomers are in the following order: L = Cl^- (468 nm) < NO_2^- (423 nm) < MeCN (413 nm) < NO^+ (383 nm). This result can be attributed to the competing σ-donor/π-acceptor properties of the respective ligands.

Electrochemical properties

The cyclic voltammograms (CVs) of ***trans*-NO$_2$**, ***cis*-NO$_2$**, and **PP-NO$_2$** are shown in Fig. 5, and electrochemical data for these

Table 1 Crystallographic data for ***trans*-NO_2**, ***cis*-NO_2′**, and **PP-NO_2**

Complex	***trans*-NO_2**·CH_3CN	***cis*-NO_2′**·0.5CH_3CN	**PP-NO_2**·2CH_3OH
Formula	$C_{38}H_{30}F_6N_6O_2P_2Ru$	$C_{61}H_{48.5}BN_{5.5}O_2PRu$	$C_{47}H_{43}F_6N_4O_4P_3Ru$
Formula weight	879.69	1033.40	1035.83
Crystal colour, habit	Red, needle	Orange-red, platelet	Orange, block
Crystal system	Monoclinic	Triclinic	Monoclinic
Crystal size, mm^3	0.30 × 0.05 × 0.05	0.15 × 0.15 × 0.10	0.15 × 0.10 × 0.05
Space group	$P2_1/n$	$P\bar{1}$	$P2_1/c$
a, Å	12.1909(17)	10.2764(2)	17.1049(6)
b, Å	11.9003(17)	21.2343(4)	13.0763(6)
c, Å	25.260(4)	24.3802(4)	20.1547(8)
α, °	90	77.0060(10)	90
β, °	99.579(3)	78.9530(10)	106.853(3)
γ, °	90	74.9360(10)	90
V, $Å^3$	3613.5(9)	4955.30(16)	4314.4(3)
Z	4	4	4
D_{calc}, g cm^{-3}	1.617	1.385	1.595
μ, mm^{-1}	0.599	0.400	0.552
$F(000)$	1776	2132	2112
R_1 [a]	0.0596	0.0337	0.0397
wR_2 [b]	0.1678	0.1071	0.0941
Goodness-of-fit S	1.032	1.178	1.004

[a] $R_1 = -\sum||F_o| - |F_c||/\sum|F_o|$. [b] $wR_2 = [\sum(w(F_o^2 - F_c^2)^2)/\sum w(F_o^2)^2]^{1/2}$.

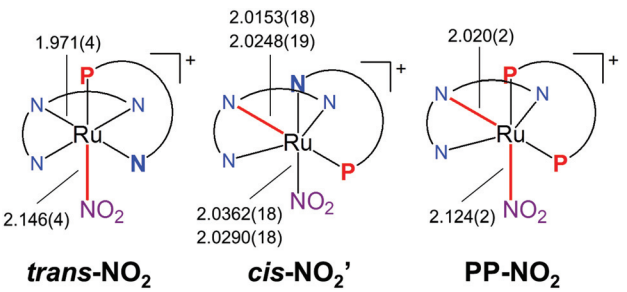

Fig. 2 Comparison of bond distances (Å) around the ruthenium centres of ***trans*-NO_2**, ***cis*-NO_2′**, and PP-NO_2.

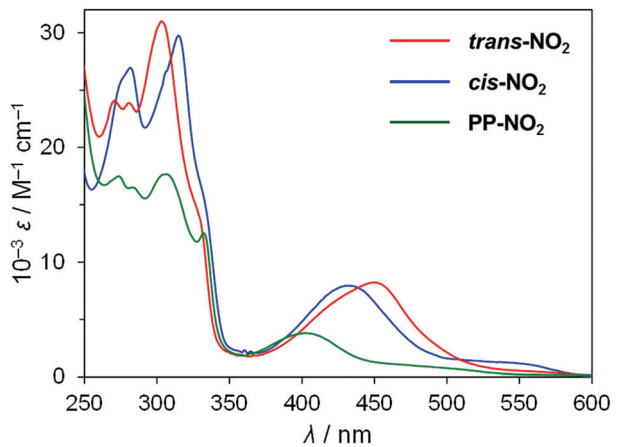

Fig. 3 UV-Vis absorption spectra of ***trans*-NO_2**, ***cis*-NO_2**, and PP-NO_2 in acetonitrile at room temperature.

complexes and related compounds are listed in Table 4. The CVs were measured in 0.1 M tetraethylammonium perchlorate (TEAP)/acetonitrile. ***cis*-NO_2** displayed one reversible oxidation wave in the positive region at $E_{1/2}$ = 0.79 V *vs.* ferrocene/ferrocenium (Fc/Fc^+), which was assigned to a Ru(III)/Ru(II) redox couple. By contrast, ***trans*-NO_2** and **PP-NO_2** exhibited one irreversible (E_{pa} = 0.79 for ***trans*-NO_2** and 0.95 V for **PP-NO_2**) and one reversible ($E_{1/2}$ = 0.97 for ***trans*-NO_2** and 1.27 V for **PP-NO_2**) redox waves in the positive region. The former irreversible oxidation peak can be attributed to oxidation of the $(Ru–NO_2)^+$ centre, and the latter reversible wave was observed exactly at the same potential as the Ru(III)/Ru(II) redox couple of the corresponding acetonitrile complex ($E_{1/2}$ = 0.97 for ***trans*-MeCN** and 1.27 V for **PP-MeCN**, Table 4 and Fig. S10b and S10d in the ESI†).[21] These observations suggest that the one-electron oxidation of ***trans*-NO_2** and **PP-NO_2** results in the release of NO_2, owing to the labilising effect of the *trans*-phosphine in each case. This leads to the formation of the respective ruthenium(II) acetonitrile complexes, which are oxidised reversibly on further sweep to more positive potential (Scheme 3). In the absence of a *trans*-labilising phosphine, the oxidation of the $(Ru–NO_2)^+$ centre of ***cis*-NO_2** occurs at a similar potential to the *trans*-isomer, but reversibly (Fig. 5 and Table 4).

In the negative potential region, ***cis*-NO_2** displayed two reversible reduction waves at −1.70 and −1.99 V, which were assigned to the trpy/$trpy^-$ and Pqn/Pqn^- redox couple, respectively. ***trans*-NO_2** exhibited two redox waves at $E_{1/2}$ = −1.77 and −2.13 V, and these redox potentials were the same as that of ***trans*-MeCN** (Table 4 and Fig. S10a in the ESI†). **PP-NO_2** displayed two irreversible waves (E_{pc} = −1.70 V and E_{pa} = −1.47 V) and one reversible ($E_{1/2}$ = −2.49 V) redox wave in the negative region. The reversible wave at $E_{1/2}$ = −2.49 V and the

Table 2 UV-Vis absorption data (λ_{max}/nm (10^{-3} ε/M^{-1} cm^{-1})) in acetonitrile and infrared data (ν/cm^{-1}) for ***trans*-NO_2**, ***cis*-NO_2**, **PP-NO_2**, and related compounds at room temperature

Complex	λ_{max}	IR	
		$\nu_{as}(NO_2)$	$\nu_s(NO_2)$
***trans*-NO_2**	443 (8.02), 327[c], 303 (31.0), 281 (23.9), 271 (24.1)	1349	1304
***cis*-NO_2**	431 (7.95), 331[c], 315 (29.7), 282 (26.9), 276[c]	1339	1286
PP-NO_2	402 (3.82), 332 (12.6), 307 (17.7), 283 (16.5), 273 (17.5)	1354	1311
$[Ru(trpy)(bpy)(NO_2)]PF_6$ [a]	472	[d]	[d]
$[Ru(trpy)(bpm)(NO_2)]PF_6$ [b]	470 (6.50), 362 (6.10), 330[c], 308 (25.6), 264 (23.3)	1342	1286

[a] Ref. 26. [b] Ref. 25. [c] Absorption shoulder. [d] Data not collected.

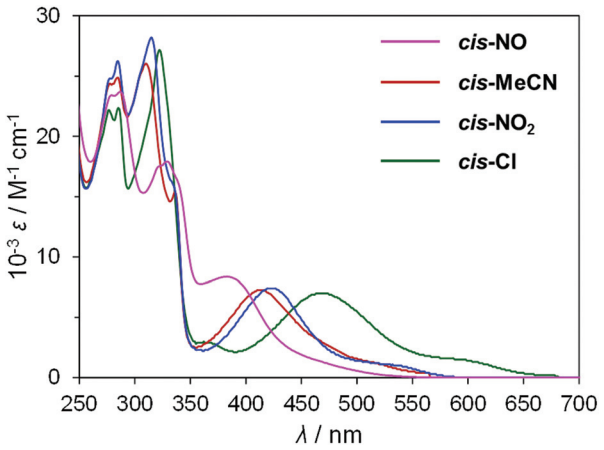

Fig. 4 UV-Vis absorption spectra of *cis*(P,X)-$[Ru(trpy)(Pqn)(L)]^n$ (L = Cl^-, NO_2^-, MeCN, NO^+) in ethylene glycol at room temperature.

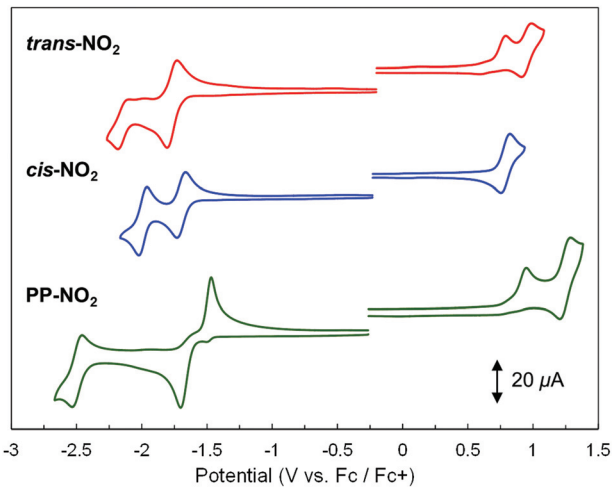

Fig. 5 Cyclic voltammograms of ***trans*-NO_2**, ***cis*-NO_2**, and **PP-NO_2** (0.5 mM) in 0.1 M TEAP/acetonitrile under an Ar atmosphere (WE: GC, CE: Pt wire, RE: Ag/Ag^+; scan rate: 100 mV s^{-1}).

irreversible anodic wave at E_{pa} = −1.47 V were similar to those observed for **PP-MeCN** (Table 4 and Fig. S10c in the ESI†). These redox behaviours of ***trans*-NO_2** and **PP-NO_2** revealed that the reduction of these complexes induced the dissociation of NO_2^- and the formation of MeCN-coordinated species; this behaviour was similar to that observed in the positive potential region. The electrochemical behaviours of the nitrito-κ*N* complexes are summarised in Scheme 3.

***cis*-NO** displayed one reversible redox wave at $E_{1/2}$ = 0.05 V and one irreversible reduction peak at E_{pc} = −0.61 V (Fig. 6). Comparison with similar nitrosyl compounds[24,25] revealed that the former redox wave was attributed to the $NO^+/NO^\bullet$ redox couple and the latter peak could be assigned to the reduction of $NO^\bullet$ to NO^-. Note that a Ru(III)/Ru(II) redox couple was not observed in the potential region between −1.6 and 1.5 V due to the low HOMO energy level originating from the poor donating ability of the NO^+ ligand.

Cyclic voltammograms of *cis*-isomers with various ligands L are shown in Fig. 7. The redox potentials of a Ru(III)/Ru(II) redox couple for each complex were observed at 0.49, 0.79, and 1.05 V for *cis*(P,Cl)-$[Ru(trpy)(Pqn)(Cl)]^+$ (***cis*-Cl**), ***cis*-NO_2**, and ***cis*-MeCN**, respectively. This result indicated the increase in the HOMO

Table 3 UV-Vis absorption data (λ_{max}/nm (10^{-3} ε/M^{-1} cm^{-1})) in acetonitrile, infrared data (ν/cm^{-1}), and redox potentials ($E_{1/2}$/V *vs.* Fc/Fc^+) in acetonitrile for ***cis*-NO** and related compounds at room temperature

Complex	λ_{max}	ν_{N-O}	$E_{1/2}(NO^+/NO^\bullet)$	$E_{1/2}(NO^\bullet/NO^-)$
***cis*-NO**[a]	383 (8.38), 329 (17.9), 323[d], 287 (23.7), 279[d]	1929	0.05	−0.61[e]
$[Ru(trpy)(bpm)(NO)](PF_6)_3$ [b]	362 (5.12), 331[d], 312[d], 291 (8.93), 265 (10.8)	1957	0.17	−0.47
trans(P,P)-$[Ru(trpy)(PPh_3)_2(NO)](ClO_4)_3$ [c]	393[d], 330 (32)	1900	0.12	[f]

[a] UV-Vis absorption data and redox potentials in ethylene glycol and γ-butyrolactone, respectively. [b] Ref. 25. [c] Ref. 24. [d] Absorption shoulder. [e] E_{pc} value for the irreversible process. [f] Data not collected.

Table 4 Redox potentials (V *vs.* Fc/Fc^+) in acetonitrile for ***trans*-NO_2**, ***cis*-NO_2**, **PP-NO_2**, and related compounds at room temperature

Complex	Red.			Ox.	
	E(1)	*E*(2)	*E*(3)	*E*(1)	*E*(2)
***trans*-NO_2**	−1.77[b]		−2.13[e,g]	0.79[c,f]	0.97[g]
***cis*-NO_2**	−1.70	−1.99	—	0.79	—
PP-NO_2	−1.70[b,e]		−2.49[g]	0.95[c,f]	1.27[g]
***trans*-MeCN**[a]	−1.70	−1.77	−2.13	0.97	—
***cis*-MeCN**[a]	[d]	[d]	[d]	1.05	—
PP-MeCN[a]	−1.50	−1.46	−2.49	1.27	—

[a] Ref. 21. [b] These reductions induced the dissociation of NO_2^- and the formation of MeCN-coordinated species. [c] NO_2 was released upon these oxidation processes, and subsequent coordination of MeCN resulted in the formation of corresponding acetonitrile complexes. [d] ***cis*-MeCN** underwent isomerization to ***trans*-MeCN** upon reduction. [e] E_{pc} values for the irreversible processes. [f] E_{pa} values for the irreversible processes. [g] Redox processes correspond to MeCN-coordinated complexes.

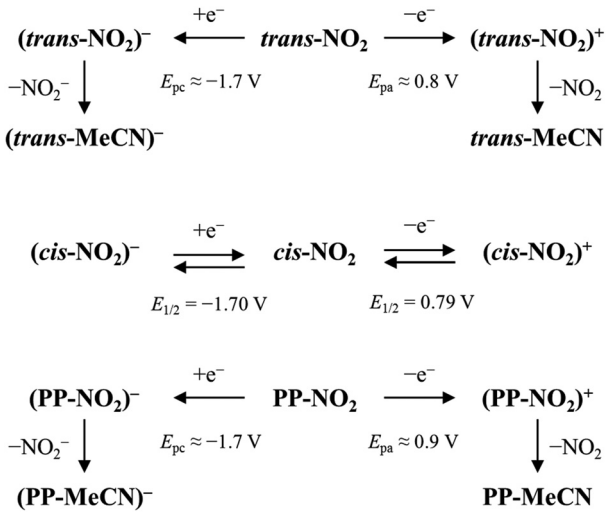

Scheme 3 Electrochemical behaviour of nitrito-κ*N* complexes.

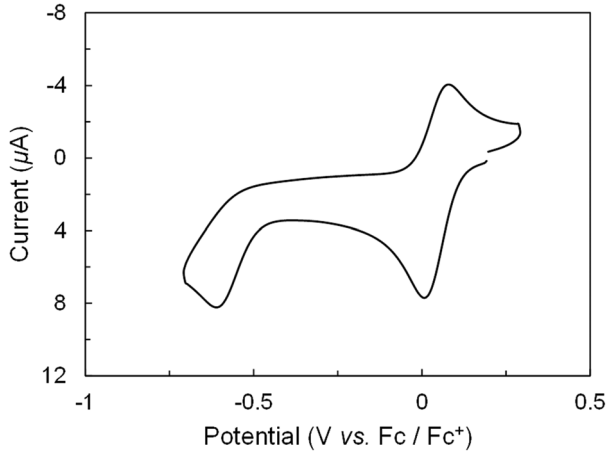

Fig. 6 Cyclic voltammogram of ***cis*-NO** (0.5 mM) in 0.1 M TEAP/γ-butyrolactone under an Ar atmosphere (WE: GC, CE: Pt wire, RE: Ag/Ag^+; scan rate: 100 mV s^{-1}).

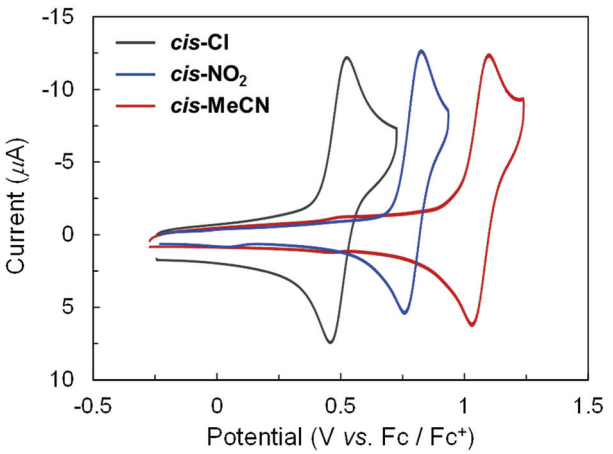

Fig. 7 Cyclic voltammograms of ***cis*-Cl**, ***cis*-NO_2**, and ***cis*-MeCN** (0.5 mM) in 0.1 M TEAP/acetonitrile under an Ar atmosphere (WE: GC, CE: Pt wire, RE: Ag/Ag^+; scan rate: 100 mV s^{-1}).

energy level by electron donation from monodentate ligands and was consistent with the UV-vis absorption spectroscopy.

Photostability of a nitrosyl complex

The photostability of ***cis*-NO** was investigated by UV-vis absorption spectroscopy and by using a Sievers nitric oxide analyser (NOA) to evaluate NO release. When a solution of ***cis*-NO** in ethylene glycol (0.05 mM) was irradiated at λ_{irr} = 355 nm, the slow spectral changes seen in Fig. 8 were observed. The quantum yields of NO release, Φ_{NO}, were quite low, 0.0048 in air saturated solution and 0.003 under helium (ESI Fig. S11 and S12†). These Φ_{NO} values are about two orders of magnitude smaller than that measured by Silva *et al.* for the photolysis of the analogous ruthenium nitrosyl complex, $[Ru(tpy)(bpy)(NO)]^{3+}$ (bpy = 2,2′-bipyridine).[27] Notably, exhaustive photolysis led to a nearly quantitative conversion to a spectrum analogous to that of ***trans*-L** (L = solvent, see Fig. S13 in the ESI†), which suggests that the photodissociation of NO and the isomerization of the complex from *cis* to *trans* form proceeds in a step-wise manner. The result is consistent with the multi-step spectral change shown in Fig. 8. It should further be noted that a Ru(II) complex, rather than the Ru(III) species is obtained upon NO photodissociation from ***cis*-NO** (ESI Fig. S13†). There are several possible explanations, one being that the Ru(III) intermediate is readily reduced by the solvent. Another is that the principal photo-reaction is release of NO^+ rather than NO[27] owing to phosphine stabilization of the low-valent Ru(II) state. However, this question was not explored in greater detail.

Substitution lability of nitrogen oxide

The substitution lability of the monodentate ligand L in the $[Ru(TL)(BL)(L)]^{n+}$-type complexes is an important factor in

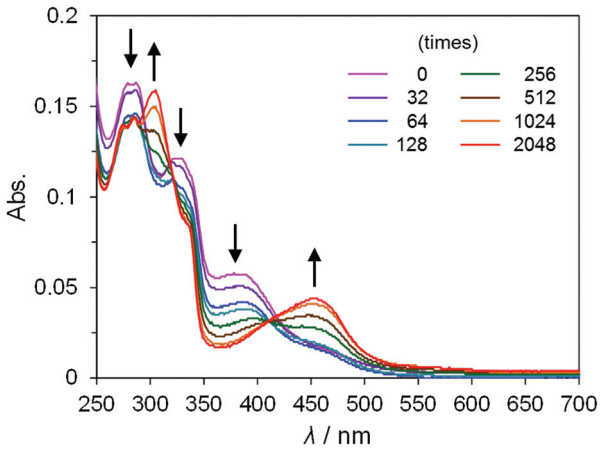

Fig. 8 UV-Vis absorption spectra of ***cis*-NO** in ethylene glycol at room temperature during photolysis using a Nd/YAG laser operating at 355 nm. "Times" indicates the number of the laser pulses used to irradiate the sample.

(a) NO_2 complex

$(trans\text{-}NO_2)^-$ ⟵ (+e⁻) *trans*-NO_2 ⟶ (−e⁻) $(trans\text{-}NO_2)^+$

labile inert labile

$(cis\text{-}NO_2)^-$ ⇄ (+e⁻) *cis*-NO_2 ⇄ (−e⁻) $(cis\text{-}NO_2)^+$

inert inert inert

(b) MeCN complex

$(trans\text{-}MeCN)^-$ ⇄ (+e⁻) *trans*-MeCN ⇄ (−e⁻) $(trans\text{-}MeCN)^+$

labile

$(cis\text{-}MeCN)^-$ ⟵ (+e⁻) *cis*-MeCN ⇄ (−e⁻) $(cis\text{-}MeCN)^+$

labile inert

Scheme 4 Changes in lability upon oxidation or reduction.

determining the reactivity of the complexes in various catalytic and photo-induced reactions. Several experimental results described above enabled us to discuss in detail the lability of the monodentate ligand in the complexes. First, the reaction of ***cis*-NO_2** with HPF_6 afforded the desired ***cis*-NO**. However, similar reactions of ***trans*-NO_2** and **PP-NO_2** resulted in the formation of ***trans*-MeCN** and **PP-MeCN** *via* the dissociation of a monodentate labile ligand, N(O)OH or NO^+ (probably the former). Second, UV-vis absorption spectroscopy revealed that the nitrito ligands of ***trans*-NO_2**, ***cis*-NO_2**, and **PP-NO_2** did not dissociate, even in strongly coordinating solvents such as acetonitrile, whereas ligand exchange reactions of ***trans*-MeCN** and **PP-MeCN** easily occurred under analogous conditions (Fig. S14 in the ESI†). ***cis*-NO** was not stable in coordinating solvent and was easily converted to a solvent-coordinated form (Fig. S4 in the ESI†).

The difference in lability of the oxidised and reduced state can also be clarified by the results of the electrochemical measurements. In the one-electron oxidised states, ***trans*-NO_2** and **PP-NO_2** were labile and were converted to the solvent-coordinated forms, ***trans*-MeCN** and **PP-MeCN**, respectively. By contrast, ***cis*-NO_2** was inert during the oxidation process, and a reversible redox wave was observed in the electrochemical measurement. Similarly, in the reduced states, the nitrito ligands of ***trans*-NO_2**, and **PP-NO_2** easily dissociated, although ***cis*-NO_2** was stable during the whole electrochemical process. However, this stability of ***cis*-NO_2** was quite different from that of ***cis*-MeCN**: the acetonitrile ligand of ***cis*-MeCN** became labile upon reduction, and the dissociation of the ligand resulted in the isomerisation of ***cis*-MeCN** to ***trans*-MeCN**.[21] The stability of the monodentate labile site for each complex is shown in Scheme 4.

The difference in the lability of these complexes can be explained by considering the following factors. First, the σ-donor character of the phosphine group significantly elongates the bond length between the ruthenium centre and the ligand *trans* to the phosphine group. This *trans* influence of the phosphine group was clearly observed in the X-ray structure for the series of nitrito-κ*N* complexes; the bond distances between the ruthenium and nitrogen atom of the nitrite ligand are 2.141(3), 2.124(2), and *ca.* 2.03 Å for ***trans*-NO_2**, **PP-NO_2**, and ***cis*-NO_2**, respectively. Therefore, the *trans*-isomers and PP complexes exhibited greater lability compared with the corresponding *cis*-isomers. Second, the electron donation from labile ligands can stabilise Ru–L bonds. The donating ability of labile ligands was confirmed by the comparison of the HOMO energy levels obtained from the electrochemical measurements of the *cis*-isomers and follows the order NO_2^- > MeCN > NO^+ and was in accordance with the stability of the complexes. Third, oxidation decreases the electron density of the Ru centre, and the π back-donating ability of Ru centres should be weakened. DFT calculations revealed that π back-donation from Ru to the nitrito ligand occurs and stabilises the Ru–L bond (Fig. S6 in the ESI†). Finally, the reduction of the complexes stabilises the five-coordinated species, as rationalised for the Ru(II)–MeCN complexes in our previous report.[21] The formation of five-coordinated species in MeCN results in ligand exchange in ***trans*-NO_2** and **PP-NO_2** or isomerisation of ***cis*-MeCN** to ***trans*-MeCN**, whereas no observable chemical process exists in the case of ***trans*-MeCN** and **PP-MeCN**. These results suggest that the (1) number and position of P atom(s), (2) coordinating ability of the monodentate ligand, and (3) oxidation state of the complexes are all factors in defining the lability of complexes.

Conclusions

This study describes the syntheses, crystal structures and spectroscopic and electrochemical properties of a series of phos-

phine-substituted ruthenium(II) polypyridine complexes with nitrogen oxides. Three nitrito-κ*N* complexes, ***trans*-NO$_2$**, ***cis*-NO$_2$**, and **PP-NO$_2$**, were synthesised by the reaction of the corresponding acetonitrile complex with $NaNO_2$ in an ethanol/water mixed solution, and a nitrosyl complex, ***cis*-NO**, was obtained by the reaction of ***cis*-NO$_2$** with HPF_6 in acetone. Crystallographic, spectroscopic, and electrochemical analyses for these complexes revealed that the σ-donating and π-accepting characters of the phosphine ligands clearly affected the dσ and dπ orbitals of the ruthenium centre, respectively. The investigation of the substitution lability of the monodentate ligand of each complex suggested that the (1) number and position of the phosphine groups, (2) coordinating ability of the monodentate ligand, and (3) oxidation state of the metal centre are all factors in determining the lability of the complex. As a further extension of our studies, investigations on various catalytic and photo-induced reactions of the phosphine-substituted ruthenium(II) polypyridine complexes are in progress in our laboratories.

Experimental

Materials

$NaNO_2$ was purchased from Kanto Chemical Co., Inc. NH_4PF_6 and HPF_6 were purchased from Wako Pure Chemical Industries, Ltd. All solvents and reagents were of the highest quality available and were used as received. *cis*(P,Cl)-[Ru(trpy)(Pqn)Cl]PF_6 (***cis*-Cl**), *trans*(P,MeCN)- and *cis*(P,MeCN)-[Ru(trpy)(Pqn)(MeCN)]$(PF_6)_2$ (***trans*-MeCN** and ***cis*-MeCN**), and [Ru(trpy)(dppbz)(MeCN)]$(PF_6)_2$ (**PP-MeCN**) were prepared following methods found in the literature.[21]

Measurements

^{1}H and ^{31}P{^{1}H} NMR spectra were recorded at room temperature on a JEOL JNM-LA500 spectrometer using tetramethylsilane as an internal reference for the ^{1}H NMR spectra and phosphoric acid as an external reference for the ^{31}P{^{1}H} NMR spectra. UV-vis absorption spectra were obtained on a Shimadzu UV-2450SIM spectrophotometer at room temperature. Elemental analyses were carried out on a Yanagimoto MT-5 elemental analyser. Infrared data were obtained using a Perkin-Elmer Spectrum 100 FT-IR spectrometer. ESI-TOF mass spectra were recorded on a JEOL JMS-T100LC mass spectrometer. All the ESI-TOF mass spectrometric measurements were recorded in the positive ion mode at a cone voltage of 20 V. Typically, each sample solution was introduced in the spectrometer at a flow rate of 10 mL min^{-1} using a syringe pump. Cyclic voltammograms were measured at room temperature on a BAS ALS Model 650DKMP electrochemical analyser in acetonitrile ([complex] = 0.5 mM; 0.1 M tetraethylammonium perchlorate (TEAP)). A glassy carbon disk, platinum wire, and Ag/Ag$^+$ electrode (Ag/0.01 M $AgNO_3$) were used as the working, auxiliary, and reference electrodes, respectively. The redox potentials of the samples were calibrated against the redox signal for the ferrocene/ferrocenium (Fc/Fc$^+$) couple. The photochemical experiments shown in Fig. 8 were made using a photolysis apparatus consisting of a LS-2134UTF Nd/YAG laser (Tokyo Instruments, INC.) with excitation provided by the third harmonic at λ = 355 nm. The pulse width was 5 ns, the beam diameter incident on the sample was 6 mm, and the repetition rate was 5 Hz.

Synthetic procedures

Synthesis of *trans*(P,NO$_2$)-[Ru(trpy)(Pqn)(NO$_2$)]PF_6 (*trans*-NO$_2$). A mixture of ***trans*-MeCN** (26.8 mg, 0.0252 mmol) and $NaNO_2$ (38.8 mg, 0.562 mmol) in ethanol (4 cm^3)/water (4 cm^3) was heated at 100 °C for 3 hours and then cooled to room temperature. Acetonitrile (2 cm^3) and a NH_4PF_6 (188.4 mg, 1.16 mmol)/water (2 cm^3) solution was added to the above-mentioned solution. The resulting red solution was concentrated to *ca.* 5 cm^3 under reduced pressure. The red product was collected by filtration and washed with water and diethyl ether. Yield 19.1 mg (0.0216 mmol, 86%). Single red crystals suitable for X-ray crystallography were grown by the slow diffusion of diethyl ether into a mixture of methanol and a few drops of acetonitrile solution of ***trans*-NO$_2$**. ESI-TOF MS (positive ion, acetonitrile): *m*/*z* 694 ([Ru(trpy)(Pqn)(NO$_2$)]$^+$). ^{1}H NMR (CD_3CN): δ 6.56 (t, 2H, *J* = 9.0 Hz), 6.98 (t, 4H, *J* = 7.0 Hz), 7.14 (t, 2H, *J* = 7.0 Hz), 7.21 (t, 2H, *J* = 8.0 Hz), 7.65 (d, 2H, *J* = 5.0 Hz), 7.80 (t, 2H, *J* = 8.0 Hz), 7.91 (m, 3H), 8.03 (d, 2H, *J* = 8.0 Hz), 8.09 (t, 1H, *J* = 7.5 Hz), 8.23 (d, 2H, *J* = 8.0 Hz), 8.46 (d, 1H, *J* = 7.0 Hz), 8.75 (d, 1H, *J* = 8.0 Hz), 9.93 (d, 1H, *J* = 5.0 Hz). ^{31}P{^{1}H} NMR (CD_3CN): δ 53.10 (s). FT-IR: $\nu_s(NO_2)$ 1304, $\nu_{as}(NO_2)$ 1349 cm^{-1}. Anal. Found: C, 48.50; H, 3.59; N, 8.22. Calcd for $C_{36}H_{32}F_6N_5O_{4.5}P_2Ru$ (***trans*-NO$_2$**·2.5H_2O): C, 48.93; H, 3.65; N, 7.93.

Synthesis of *cis*(P,NO$_2$)-[Ru(trpy)(Pqn)(NO$_2$)]PF_6 (*cis*-NO$_2$). This complex was prepared from ***cis*-MeCN** (26.0 mg, 0.0250 mmol) instead of ***trans*-MeCN** by a method similar to that for ***trans*-NO$_2$**. Yield 19.5 mg (0.0221 mmol, 88%). ESI-TOF MS (positive ion, acetonitrile): *m*/*z* 694 ([Ru(trpy)(Pqn)(NO$_2$)]$^+$). ^{1}H NMR (CD_3CN): δ 6.81 (t, 2H, *J* = 6.5 Hz), 7.06 (m, 1H), 7.4 1 (d, 2H, *J* = 5.5 Hz), 7.52 (m, 4H), 7.63 (t, 2H, *J* = 7.5 Hz), 7.73 (m, 4H), 7.84 (t, 2H, *J* = 8.0 Hz), 7.92 (d, 1H, *J* = 5.5 Hz), 7.97 (t, 1H, *J* = 7.5 Hz), 8.18 (d, 1H, *J* = 8.0 Hz), 8.23 (d, 1H, *J* = 8.0 Hz), 8.36 (m, 3H), 8.55 (d, 2H, *J* = 8.0 Hz) 8.78 (t, 1H, *J* = 8.0 Hz). ^{31}P{^{1}H} NMR (CD_3CN): δ 54.06 (s). FT-IR: $\nu_s(NO_2)$ 1286, $\nu_{as}(NO_2)$ 1339 cm^{-1}. Anal. Found: C, 50.38; H, 3.44; N, 8.19. Calcd for $C_{36}H_{29}F_6N_5O_3P_2Ru$ (***cis*-NO$_2$**·H_2O): C, 50.47; H, 3.41; N, 8.18.

Synthesis of *cis*(P,NO$_2$)-[Ru(trpy)(Pqn)(NO$_2$)]BPh_4 (*cis*-NO$_2$′). This complex was prepared by a method similar to that for ***cis*-NO$_2$** with an excess of $NaBPh_4$ instead of NH_4PF_6. The product was recrystallised from dichloromethane and a small amount of acetonitrile/diethyl ether to afford orange-red crystals of ***cis*-NO$_2$′**. Anal. Found: C, 70.54; H, 4.72; N, 6.92. Calcd for $C_{60}H_{48}BN_5O_{2.5}PRu$ (***cis*-NO$_2$′**·0.5H_2O): C, 70.52; H, 4.73; N, 6.85.

Synthesis of *cis*(P,NO)-[Ru(trpy)(Pqn)(NO)](PF$_6$)$_3$ (*cis*-NO). ***cis*-NO$_2$** (22.4 mg, 0.0261 mmol) was dissolved in acetone (1 cm^3). An excess of 60% HPF_6 acid solution was added dropwise until the solution changed colour from red to yellow with the shielding of light in an ice-water bath. The resulting yellow solution was concentrated under reduced pressure, and 10 cm^3 of diethyl ether was added to precipitate the product. Yield 27.4 mg (0.0223 mmol, 85%). ^{1}H NMR (acetone-d_6): δ 7.47 (t, 2H, J = 7.0 Hz), 7.66 (m, 1H), 7.80 (d, 2H, J = 6.0 Hz), 7.86 (m, 4H), 8.01 (t, 2H, J = 7.5 Hz), 8.12 (dd, 4H, J = 7.5, 13.0 Hz), 8.42 (t, 1H, J = 7.5 Hz), 8.49 (m, 2H), 8.55 (m, 1H), 8.80 (d, 1H, J = 8.0 Hz), 9.01 (m, 3H), 9.10 (m, 1H), 9.22 (m, 3H). ^{31}P{^{1}H} NMR (acetone-d_6): δ 54.23 (s). FT-IR: ν_s(NO) 1929 cm^{-1}. Anal. Found: C, 35.03; H, 2.95; N, 5.59. Calcd for $C_{36}H_{40}F_{18}N_5O_{7.5}P_4Ru$ (***cis*-NO**·6.5H_2O): C, 35.16; H, 3.28; N, 5.70.

Synthesis of [Ru(trpy)(dppbz)(NO$_2$)]PF$_6$ (PP-NO$_2$). This complex was prepared from **PP-MeCN** (31.5 mg, 0.0263 mmol) instead of ***trans*-MeCN** by a method similar to that for ***trans*-NO$_2$**. Yield 22.9 mg (0.0227 mmol, 86%). Single orange crystals suitable for X-ray crystallography were grown through the slow diffusion of diethyl ether into a mixture of methanol and a few drops of acetonitrile solution of **PP-NO$_2$**. ESI-TOF MS (positive ion, acetonitrile): m/z 827 ([Ru(trpy)(dppbz)(NO$_2$)]$^+$). ^{1}H NMR (CD_3CN): δ 6.50 (m, 4H), 6.78 (m, 2H), 6.88 (m, 4H), 7.08 (d, 2H, J = 5.5 Hz), 7.17 (m, 2H), 7.45 (t, 4H, J = 7.5 Hz), 7.61 (m, 7H), 7.77 (m, 3H), 7.87 (t, 1H, J = 7.5 Hz), 8.03 (d, 2H, J = 8.0 Hz), 8.23 (m, 3H), 8.39 (t, 1H, J = 7.5 Hz). ^{31}P{^{1}H} NMR (CD_3CN): δ 62.65 (d, $^2J_{P-P}$ = 14.2 Hz), 68.59 (d, $^2J_{P-P}$ = 14.2 Hz). FT-IR: ν_s(NO$_2$) 1311, ν_{as}(NO$_2$) 1354 cm^{-1}. Anal. Found: C, 53.62; H, 4.05; N, 5.46. Calcd for $C_{45}H_{39}F_6N_4O_4P_3Ru$ (**PP-NO$_2$**·2H_2O): C, 53.63; H, 3.90; N, 5.56.

X-ray crystallography

The X-ray data collection and processing was performed on a Kappa APEX II CCDC diffractometer by using graphite-monochromated Mo-Kα radiation (0.71075 Å) for ***trans*-NO$_2$** and **PP-NO$_2$**. Single-crystal X-ray diffraction measurement of ***cis*-NO$_2$′** was performed with a RAXIS-RAPID Imaging Plate diffractometer equipped with confocal monochromated Mo-Kα (0.71075 Å) radiation, and the data were processed using RAPID-AUTO (Rigaku). The structure was solved by the direct methods using SIR-92[28] and refined on F^2 with the full-matrix least squares technique using SHELXL-2014.[29] All non-hydrogen atoms were refined anisotropically. Molecular graphics were generated using ORTEP-3 for Windows[30] and POV-RAY.[31] A summary of the crystallographic data and structure refinement parameters is given in Table 1.

The crystallographic data have been deposited at the Cambridge Crystallographic Data Centre: deposition numbers CCDC 1040452, 1040453, and 1040454 for ***trans*-NO$_2$**, ***cis*-NO$_2$′**, and **PP-NO$_2$**, respectively.

DFT calculations

Calculations were performed using the DFT method implemented in the Gaussian 09 package.[32] The structures were fully optimised using the hybrid B3LYP method, which uses Becke's three-parameter exchange functional[33] with the correlation energy functional of Lee, Yang, and Parr.[34] All calculations were performed using the standard double-ζ type LANL2DZ basis set[35a–c] or SDD basis set[35d] implemented in Gaussian 09, without adding any extra polarisation or diffuse functions. The LANL2DZ basis set also uses a relativistic effective core potential (RECP) for the Ru atom to account for the scalar relativistic effects of the inner 28 core electrons ([Ar] 3d^{10}). All calculations were performed using the polarisable continuum model (PCM)[36] to compute the structures in acetonitrile media. All stationary points were characterised as minima of the potential energy surface by their harmonic vibrational frequencies. The free energies at 298 K and 1 atm were obtained through thermochemical analysis of the frequency calculation using the thermal correction to Gibbs free energy as implemented in Gaussian 09. The excited states were calculated using the TDDFT[37] method within the Tamm–Dancoff approximation as implemented in Gaussian 09. These calculations employ the hybrid B3LYP functional along with the basis sets described above. A minimum of 100 excited states was computed in each calculation. To obtain the simulated spectrum of each species, transition energies and oscillator strengths were interpolated by a Gaussian convolution with a common σ value of 0.2 eV.

Quantum yield measurements

Nitric oxide was detected and analysed using a GE Sievers model 280i nitric oxide analyser (NOA).[38] Known volumes of the gases from the solution headspace were injected into the NOA purge vessel, and these gases were entrained to the detector using helium or medical grade air. The NO present in the sample was quantified using a calibration curve generated from the reaction of $NaNO_2$ with acidic KI. Chemical actinometry was performed with ferric oxalate solutions.[39] The photolysis source was the output from a 200 W high-pressure mercury lamp passed through an IR filter and collimated with lenses. An appropriate interference filter was used to select the desired λ_{irr}. A shutter shielded the sample from the arc lamp. A sample of a known volume in a 1 cm square cuvette with a magnetic stirring bar was irradiated for determined time periods.[40] The NO quantum yields (Φ_{NO}) were calculated based on the nitric oxide release measured using the NOA.

Acknowledgements

This work was supported by a Grant-in-Aid for Young Scientists (A) (No. 25708011) (to S.M.), a Grant-in-Aid for Challenging Exploratory Research (No. 26620160) (to S.M.), and a Grant-in-Aid for Young Scientists (A) (No. 15H05480) (to M.K) from the Japan Society for the Promotion of Science. This work was also supported by a Grant-in-Aid for Scientific Research on Innovative Areas "AnApple" (No. 25107526). Studies at UCSB were supported by a US National Foundation Grant (CHE-1058794 and CHE-1405062). We thank Dr Guang Wu of UCSB for the

X-ray diffraction studies and Dr John Garcia of UCSB for confirming photochemical results.

Notes and references

1 (*a*) N. Sutin, *J. Photochem.*, 1979, **10**, 19–40; (*b*) K. Kalyanasundaram, *Coord. Chem. Rev.*, 1982, **46**, 159–244; (*c*) E. S. Dodsworth and A. B. P. Lever, *Chem. Phys. Lett.*, 1986, **124**, 152–158; (*d*) A. Juris, V. Balzani, F. Barigelletti, S. Campagna, P. Belser and A. von Zelewsky, *Coord. Chem. Rev.*, 1988, **84**, 85–277; (*e*) A. B. P. Lever, *Inorg. Chem.*, 1990, **29**, 1271–1285; (*f*) V. Balzani and A. Juris, *Coord. Chem. Rev.*, 2001, **211**, 97–115; (*g*) D. W. Thompson, J. F. Wishart, B. S. Brunschwig and N. Sutin, *J. Phys. Chem. A*, 2001, **105**, 8117–8122; (*h*) S. Campagna, F. Puntoriero, F. Nastasi, G. Bergamini and V. Balzani, *Top. Curr. Chem.*, 2007, **280**, 117–214; (*i*) T. P. Yoon, M. A. Ischay and J. Du, *Nat. Chem.*, 2010, **2**, 527–532; (*j*) Q. Sun, S. Mosquera-Vazquez, Y. Suffren, J. Hankache, N. Amstutz, L. M. L. Daku, E. Vauthey and A. Hauser, *Coord. Chem. Rev.*, 2015, **282–283**, 87–99.

2 (*a*) C. D. Clark and M. Z. Hoffman, *Coord. Chem. Rev.*, 1997, **159**, 359–373; (*b*) L. De Cola and P. Belser, *Coord. Chem. Rev.*, 1998, **177**, 301–346; (*c*) M. D. Ward and F. Barigelletti, *Coord. Chem. Rev.*, 2001, **216–217**, 127–154; (*d*) M. H. V. Huynh, D. M. Dattelbaum and T. J. Meyer, *Coord. Chem. Rev.*, 2005, **249**, 457–483; H. Kon, K. Tsuge, T. Imamura, Y. Sasaki, S. Ishizaka, N. Kitamura and M. Kato, *Dalton Trans.*, 2008, 1541–1543; (*e*) A. Lavie-Cambot, C. Lincheneau, M. Cantuel, Y. Leydet and N. D. McClenaghan, *Chem. Soc. Rev.*, 2010, **39**, 506–515; (*f*) O. Filevich, B. García-Acosta and R. Etchenique, *Photochem. Photobiol. Sci.*, 2012, **11**, 843–847.

3 (*a*) F. G. Gao and A. J. Bard, *J. Am. Chem. Soc.*, 2000, **122**, 7426–7427; (*b*) J. N. Demas and B. A. DeGraff, *Coord. Chem. Rev.*, 2001, **211**, 317–351; (*c*) P. D. Beer and E. J. Hayes, *Coord. Chem. Rev.*, 2003, **240**, 167–189; (*d*) R. Martinez-Máñez and F. Sancenón, *Chem. Rev.*, 2003, **103**, 4419–4476; (*e*) A. S. Polo, M. K. Itokazu and N. Y. M. Iha, *Coord. Chem. Rev.*, 2004, **248**, 1343–1361; (*f*) M. S. Vickers, K. S. Martindale and P. D. Beer, *J. Mater. Chem.*, 2005, **15**, 2784–2790; (*g*) N. Haddour, J. Chauvin, C. Gondran and S. Cosnier, *J. Am. Chem. Soc.*, 2006, **128**, 9693–9698; (*h*) H. Wei and E. Wang, *Trends Anal. Chem.*, 2008, **27**, 447–459; (*i*) J. L. Delaney, C. F. Hogan, J. Tian and W. Shen, *Anal. Chem.*, 2011, **83**, 1300–1306.

4 (*a*) G. J. Wilson, A. Launikonis, W. H. F. Sasse and A. W.-H. Mau, *J. Phys. Chem. A*, 1997, **101**, 4860–4866; (*b*) J. A. Simon, S. L. Curry, R. H. Schmehl, T. R. Schatz, P. Piotrowiak, X. Jin and R. P. Thummel, *J. Am. Chem. Soc.*, 1997, **119**, 11012–11022; (*c*) A. D. Guerzo, S. Leroy, F. Fages and R. H. Schmehl, *Inorg. Chem.*, 2002, **41**, 359–366; (*d*) D. S. Tyson, C. R. Luman, X. Zhou and F. N. Castellano, *Inorg. Chem.*, 2001, **40**, 4063–4071; (*e*) S. Bernhard, J. A. Barron, P. L. Houston, H. D. Abruña, J. L. Ruglovksy, X. Gao and G. G. Malliaras, *J. Am. Chem. Soc.*, 2002, **128**, 9693–9698; (*f*) S. Welter, K. Brunner, J. W. Hofstraat and L. D. Cola, *Nature*, 2003, **421**, 54–57; (*g*) H. Shahroosvand, P. Abbasi, A. Faghih, E. Mohajerani, M. Janghouri and M. Mahmoudi, *RSC Adv.*, 2014, **4**, 1150–1154.

5 (*a*) J. K. Barton, *Science*, 1986, **233**, 727–734; (*b*) C. Turro, S. H. Bossmann, Y. Jenkins, J. K. Barton and N. J. Turro, *J. Am. Chem. Soc.*, 1995, **117**, 9026–9032; (*c*) H. B. Gray and J. R. Winkler, *Annu. Rev. Biochem.*, 1996, **65**, 537–561; (*d*) A. D. Guerzo and A. K.-D. Mesmaeker, *Inorg. Chem.*, 2002, **41**, 938–945; (*e*) S. Le Gac, M. Foucart, P. Gerbaux, E. Defrancq, C. Moucheron and A. Kirsch-De Mesmaeker, *Dalton Trans.*, 2010, **39**, 9672–9683; (*f*) H. Song, J. T. Kaiser and J. K. Barton, *Nat. Chem.*, 2012, **4**, 615–620; (*g*) H. Niyazi, J. P. Hall, K. O'Sullivan, G. Winter, T. Sorensen, J. M. Kelly and C. J. Cardin, *Nat. Chem.*, 2012, **4**, 621–628; (*h*) A. C. Komor and J. K. Barton, *Chem. Commun.*, 2013, **49**, 3617–3630.

6 (*a*) T. J. Meyer and M. H. V. Huynh, *Inorg. Chem.*, 2003, **42**, 8140–8160; (*b*) E. Masllorens, M. Rodriguez, I. Romero, A. Roglans, T. Parella, J. Benet-Buchholz, M. Poyatos and A. Llobet, *J. Am. Chem. Soc.*, 2006, **128**, 5306–5307; (*c*) Y. Shiota, J. M. Herrera, G. Juhász, T. Abe, S. Ohzu, T. Ishizuka, T. Kojima and K. Yoshizawa, *Inorg. Chem.*, 2011, **50**, 6200–6209; (*d*) T. Kojima, K. Nakayama, K. Ikemura, T. Ogura and S. Fukuzumi, *J. Am. Chem. Soc.*, 2011, **133**, 11692–11700; (*e*) Z. Hu, H. Du, W.-L. Man, C.-F. Leung, H. Liang and T.-C. Lau, *Chem. Commun.*, 2012, **48**, 1102–1104; (*f*) Z. Hu, L. Ma, J. Xie, H. Du, W. W. Y. Lam and T.-C. Lau, *New J. Chem.*, 2013, **37**, 1707–1710.

7 (*a*) J. J. Concepcion, J. W. Jurss, J. L. Templeton and T. J. Meyer, *J. Am. Chem. Soc.*, 2008, **130**, 16462–16463; (*b*) H.-W. Tseng, R. Zong, J. T. Muckerman and R. P. Thummel, *Inorg. Chem.*, 2008, **47**, 11763–11773; (*c*) S. Masaoka and K. Sakai, *Chem. Lett.*, 2009, **38**, 182–183; (*d*) M. Yoshida, S. Masaoka and K. Sakai, *Chem. Lett.*, 2009, **38**, 702–703; (*e*) S. Romain, L. Vigara and A. Llobet, *Acc. Chem. Res.*, 2009, **42**, 1944–1953; (*f*) J. J. Concepcion, J. W. Jurss, M. K. Brennaman, P. G. Hoertz, A. O. T. Patrocinio, N. Y. Murakami Iha, J. L. Templeton and T. J. Meyer, *Acc. Chem. Res.*, 2009, **42**, 1954–1965; (*g*) L. Duan, L. Tong, Y. Xu and L. Sun, *Energy Environ. Sci.*, 2011, **4**, 3296–3313; (*h*) D. J. Wasylenko, R. D. Palmer and C. P. Berlinguette, *Chem. Commun.*, 2013, **49**, 218–227; (*i*) M. D. Kärkäs, O. Verho, E. V. Johnston and B. Åkermark, *Chem. Rev.*, 2014, **114**, 11863–12001.

8 (*a*) H. Yamazaki, T. Hakamata, M. Komi and M. Yagi, *J. Am. Chem. Soc.*, 2011, **133**, 8846–8849; (*b*) J. L. Boyer, D. E. Polyansky, D. J. Szalda, R. Zong, R. P. Thummel and E. Fujita, *Angew. Chem., Int. Ed.*, 2011, **50**, 12600–12604; (*c*) S. K. Padhi, R. Fukuda, M. Ehara and K. Tanaka, *Inorg. Chem.*, 2012, **51**, 5386–5392; (*d*) M. Hirahara, M. Z. Ertem, M. Komi, H. Yamazaki, C. J. Cramer and M. Yagi, *Inorg. Chem.*, 2013, **52**, 6354–6364.

9 (*a*) K. Tanaka and D. Ooyama, *Coord. Chem. Rev.*, 2002, **226**, 211–218; (*b*) J.-M. Savéant, *Chem. Rev.*, 2008, **108**,

2348–2378; (*c*) Y. Tsukahara, T. Wada and K. Tanaka, *Chem. Lett.*, 2010, **39**, 1134–1135; (*d*) K. Kobayashi, T. Kikuchi, S. Kitagawa and K. Tanaka, *Angew. Chem., Int. Ed.*, 2014, **52**, 1–6.

10 (*a*) Z. Chen, C. Chen, D. R. Weinberg, P. Kang, J. J. Concepcion, D. P. Harrison, M. S. Brookhart and T. J. Meyer, *Chem. Commun.*, 2011, **47**, 12607–12609; (*b*) Z. Chen, J. J. Concepcion, M. K. Brennaman, P. Kang, M. R. Norris, P. G. Hoertz and T. J. Meyer, *Proc. Natl. Acad. Sci. U. S. A.*, 2012, **109**, 15606–15611; (*c*) Z. Chen, P. Kang, M.-T. Zhang and T. J. Meyer, *Chem. Commun.*, 2014, **50**, 335–337; (*d*) P. Kang, Z. Chen, A. Nayak, S. Zhang and T. J. Meyer, *Energy Environ. Sci.*, 2014, **7**, 4007–4012.

11 (*a*) A. Kobayashi, R. Takatori, I. Kikuchi, H. Konno, K. Sakamoto and O. Ishitani, *Organometallics*, 2001, **20**, 3361–3363; (*b*) A. Kobayashi, H. Konno, K. Sakamoto, A. Sekine, Y. Ohashi, M. Iida and O. Ishitani, *Chem. – Eur. J.*, 2005, **11**, 4219–4226; (*c*) M. Kimura and K. Tanaka, *Angew. Chem., Int. Ed.*, 2008, **47**, 9768–9771; (*d*) Y. Matsubara, E. Fujita, M. D. Doherty, J. T. Muckerman and C. Creutz, *J. Am. Chem. Soc.*, 2012, **134**, 15743–15757; (*e*) Y. Matsubara, T. Kosaka, K. Koga, A. Nagasawa, A. Kobayashi, H. Konno, C. Creutz, K. Sakamoto and O. Ishitani, *Organometallics*, 2013, **32**, 6162–6165; (*f*) J. Huang, J. Chen, H. Gao and L. Chen, *Inorg. Chem.*, 2014, **53**, 9570–9580.

12 (*a*) R. W. Callahan and T. J. Meyer, *Inorg. Chem.*, 1977, 574–581; (*b*) H. Hadadzadeh, M. C. DeRosa, G. P. A. Yap, A. R. Rezvani and R. J. Crutchley, *Inorg. Chem.*, 2002, **41**, 6521–6526; (*c*) M. G. Sauaia, R. G. de Lima, A. C. Tedesco and R. S. da Silva, *J. Am. Chem. Soc.*, 2003, **125**, 14718–14719; (*d*) Z. N. da Rocha, M. S. P. Marchesi, J. C. Molin, C. N. Lunardi, K. M. Miranda, L. M. Bendhack, P. C. Ford and R. S. da Silva, *Dalton Trans.*, 2008, 4282–4287; (*e*) A. C. Pereira, P. C. Ford, R. S. da Silva and L. M. Bendhack, *Nitric Oxide*, 2011, **24**, 192–198; (*f*) T. A. Heinrich, A. C. Tedesco, J. M. Fukuto and R. S. da Silva, *Dalton Trans.*, 2014, **43**, 4021–4025; (*g*) R. G. de Lima, B. R. Silva, R. S. da Silva and L. M. Bendhack, *Molecules*, 2014, **19**, 9628–9654.

13 (*a*) T. Kinoshita, J. T. Dy, S. Uchida, T. Kubo and H. Segawa, *Nat. Photonics*, 2013, **7**, 535–539; (*b*) R. Katoh and A. Furube, *J. Photochem. Photobiol., C*, 2014, **20**, 1–16.

14 (*a*) R. Noyori and T. Ohkuma, *Angew. Chem., Int. Ed.*, 2001, **40**, 40–73; (*b*) R. Noyori, *Angew. Chem., Int. Ed.*, 2002, **41**, 2008–2022; (*c*) R. Noyori, *Adv. Synth. Catal.*, 2003, **345**, 15–32; (*d*) S. E. Clapham, A. Hadzovic and R. H. Morris, *Coord. Chem. Rev.*, 2004, **248**, 2201–2237; (*e*) A. F. Trindade, P. M. P. Gois and C. A. M. Afonso, *Chem. Rev.*, 2009, **109**, 418–514; (*f*) R. Noyori, *Angew. Chem., Int. Ed.*, 2013, **52**, 79–92.

15 (*a*) P. Schwab, M. B. France, J. W. Ziller and R. H. Grubbs, *Angew. Chem., Int. Ed. Engl.*, 1995, **34**, 2039–2041; (*b*) H. Clavier and S. P. Nolan, *Chem. – Eur. J.*, 2007, **13**, 8029–8036; (*c*) G. C. Vougioukalakis and R. H. Grubbs, *Chem. Rev.*, 2010, **110**, 1746–1787; (*d*) J. S. M. Samec, B. K. Keitz and R. H. Grubbs, *J. Organomet. Chem.*, 2010, **695**, 1831–1837; (*e*) S. P. Nolan and H. Clavier, *Chem. Soc. Rev.*, 2010, **39**, 3305–3316.

16 (*a*) C. M. Moore and N. K. Szymczak, *Chem. Commun.*, 2013, **49**, 400–402; (*b*) K.-N. T. Tseng, J. W. Kampf and N. K. Szymczak, *Organometallics*, 2013, **32**, 2046–2049; (*c*) K.-N. T. Tseng, A. M. Rizzi and N. K. Szymczak, *J. Am. Chem. Soc.*, 2013, **135**, 16352–16355.

17 (*a*) D. K. Dutta and B. Deb, *Coord. Chem. Rev.*, 2011, **255**, 1686–1712; (*b*) C. S. Yi, *J. Organomet. Chem.*, 2011, **696**, 76–80; (*c*) I. Mellone, M. Peruzzini, L. Rosi, D. Mellmann, H. Junge, M. Beller and L. Gonsalvi, *Dalton Trans.*, 2013, **42**, 2495–2501.

18 (*a*) R. A. Leising, J. J. Grzybowski and K. J. Takeuchi, *Inorg. Chem.*, 1988, **27**, 1020–1025; (*b*) B. J. Coe, D. W. Thompson, C. T. Culbertson, J. R. Schoonover and T. J. Meyer, *Inorg. Chem.*, 1995, **34**, 3385–3395; (*c*) L. F. Szczepura, S. A. Kubow, R. A. Leising, W. J. Perez, M. H. V. Huynh, C. H. Lake, D. G. Churchill, M. R. Churchill and K. J. J. Takeuchi, *Chem. Soc., Dalton Trans. Inorg. Chem.*, 1996, **7**, 1463–1470; (*d*) W. J. Perez, C. H. Lake, R. F. See, L. M. Toomey, M. R. Churchill, K. J. Takeuchi, C. P. Radano, W. J. Boyko and C. A. Bessel, *J. Chem. Soc., Dalton Trans.*, 1999, 2281–2292; (*e*) S. B. Billings, M. T. Mock, K. Wiacek, M. B. Turner, W. S. Kassel, K. J. Takeuchi, A. L. Rheingold, W. J. Boyko and C. A. Bessel, *Inorg. Chim. Acta*, 2003, **355**, 103–115; (*f*) S. Sharma, S. K. Singh, M. Chandra and D. S. Pandey, *J. Inorg. Biochem.*, 2005, **99**, 458–466.

19 (*a*) B. P. Sullivan, D. J. Salmon and T. J. Meyer, *Inorg. Chem.*, 1978, **17**, 3334–3341; (*b*) B. P. Sullivan, D. Conrad and T. J. Meyer, *Inorg. Chem.*, 1985, **24**, 3640–3645; (*c*) J. P. Otruba, G. A. Neyhart, W. J. Dressick, J. L. Marshall, B. P. Sullivan, P. A. Watkins and T. J. Meyer, *J. Photochem.*, 1986, **35**, 133–153; (*d*) R. A. Leising and K. J. Takeuchi, *Inorg. Chem.*, 1987, **26**, 4391–4393; (*e*) R. A. Leising, J. S. Ohman and K. J. Takeuchi, *Inorg. Chem.*, 1988, **27**, 3804–3809; (*f*) C. A. Bessel, J. A. Margarucci, J. H. Acquaye, R. S. Rubmo, J. Crandall, A. J. Jircitano and K. J. Takeuchi, *Inorg. Chem.*, 1993, **32**, 5779–5784; (*g*) M. R. Churchill, L. M. Krajkowski, M. H. V. Huynh and K. J. Takeuchi, *J. Chem. Crystallogr.*, 1997, **27**, 589–597; (*h*) M. Salierno, E. Marceca, D. S. Peterka, R. Yuste and R. Etchenique, *J. Inorg. Biochem.*, 2010, **104**, 418–422; (*i*) S. V. Litke, A. Y. Ershov and T. J. Meyer, *J. Phys. Chem. A*, 2011, **115**, 14235–14242; (*j*) V. S. Miguel, M. Álvarez, O. Filevich, R. Etchenique and A. del Campo, *Langmuir*, 2012, **28**, 1217–1221; (*k*) R. Araya, V. Andino-Pavlovsky, R. Yuste and R. Etchenique, *ACS Chem. Neurosci.*, 2013, **4**, 1163–1167.

20 (*a*) M. E. Marmion and K. J. Takeuchi, *J. Chem. Soc., Dalton Trans.*, 1988, 2385–2391; (*b*) C. A. Bessel, R. A. Leising and K. J. Takeuchi, *J. Chem. Soc., Chem. Commun.*, 1991, 833–835; (*c*) N. D. Schley, G. E. Dobereiner and R. H. Crabtree, *Organometallics*, 2011, **30**, 4174–4179.

21 G. Nakamura, M. Okamura, M. Yoshida, T. Suzuki, H. D. Takagi, M. Kondo and S. Masaoka, *Inorg. Chem.*, 2014, **53**, 7214–7226.
22 J. Heinecke and P. C. Ford, *Coord. Chem. Rev.*, 2010, **254**, 235–247.
23 M. T. Gladwin, A. N. Schechter, D. B. Kim-Shapiro, R. P. Patel, N. Hogg, S. Shiva, R. O. Cannon III, M. Kelm, D. A. Wink, M. Graham Espey, E. H. Oldfield, R. M. Pluta, B. A. Freeman, J. R. Lancaster Jr., M. Feelisch and J. O. Lundberg, *Nat. Chem. Biol.*, 2005, **1**, 308–314.
24 R. A. Leising, S. A. Kubow and K. J. Takeuchi, *Inorg. Chem.*, 1990, **29**, 4569–4574.
25 P. Singh, J. Fiedler, S. Záliš, C. Duboc, M. Niemeyer, F. Lissner, T. Schleid and W. Kaim, *Inorg. Chem.*, 2007, **46**, 9254–9261.
26 (*a*) D. W. Pipes and T. J. Meyer, *Inorg. Chem.*, 1984, **23**, 2466–2472; (*b*) W. R. Murphy, Jr., K. J. Takeuchi, M. H. Barley and T. J. Meyer, *Inorg. Chem.*, 1984, **25**, 1041–1053.
27 R. G. de Lima, M. G. Sauaia, D. Bonaventure, A. C. Tedesco, L. M. Bendhack and R. S. da Silva, *Inorg. Chim. Acta*, 2006, **359**, 2543–2549.
28 A. Altomare, G. Cascarano, C. Giacovazzo and A. J. Guagliardi, *J. Appl. Crystallogr.*, 1993, **26**, 343–350.
29 G. M. Sheldrick, *Acta Crystallogr., Sect. A: Found. Crystallogr.*, 2008, **64**, 112–122.
30 L. J. Farrugia, *J. Appl. Crystallogr.*, 1997, **30**, 565–566.
31 T. D. Fenn, D. Ringe and G. A. Petsko, *J. Appl. Crystallogr.*, 2003, **36**, 944–947.
32 M. J. Frisch, G. W. Trucks, H. B. Schlegel, G. E. Scuseria, M. A. Robb, J. R. Cheeseman, G. Scalmani, V. Barone, B. Mennucci, G. A. Petersson, H. Nakatsuji, M. Caricato, X. Li, H. P. Hratchian, A. F. Izmaylov, J. Bloino, G. Zheng, J. L. Sonnenberg, M. Hada, M. Ehara, K. Toyota, R. Fukuda, J. Hasegawa, M. Ishida, T. Nakajima, Y. Honda, O. Kitao, H. Nakai, T. Vreven, J. A. Montgomery, Jr., J. E. Peralta, F. Ogliaro, M. Bearpark, J. J. Heyd, E. Brothers, K. N. Kudin, V. N. Staroverov, T. Keith, R. Kobayashi, J. Normand, K. Raghavachari, A. Rendell, J. C. Burant, S. S. Iyengar, J. Tomasi, M. Cossi, N. Rega, J. M. Millam, M. Klene, J. E. Knox, J. B. Cross, V. Bakken, C. Adamo, J. Jaramillo, R. Gomperts, R. E. Stratmann, O. Yazyev, A. J. Austin, R. Cammi, C. Pomelli, J. W. Ochterski, R. L. Martin, K. Morokuma, V. G. Zakrzewski, G. A. Voth, P. Salvador, J. J. Dannenberg, S. Dapprich, A. D. Daniels, O. Farkas, J. B. Foresman, J. V. Ortiz, J. Cioslowski and D. J. Fox, *Gaussian 09 (Revision C.01)*, Gaussian, Inc., Wallingford CT, 2010.
33 A. D. Becke, *J. Chem. Phys.*, 1993, **98**, 5648–5652.
34 C. Lee, W. Yang and R. G. Parr, *Phys. Rev. B: Condens. Matter*, 1988, **37**, 785–789.
35 (*a*) T. H. Dunning, Jr. and P. J. Hay, in *Modern Theoretical Chemistry*, ed. H. F. Schaefer, III, Plenum, New York, 1976; (*b*) P. J. Hay and W. R. Wadt, *J. Chem. Phys.*, 1985, **82**, 270–283; (*c*) P. J. Hay and W. R. Wadt, *J. Chem. Phys.*, 1985, **82**, 299–310; (*d*) D. Andrae, U. Haeussermann, M. Dolg, H. Stoll and H. Preuss, *Theor. Chim. Acta*, 1990, **77**, 123.
36 M. Cossi, G. Scalmani, N. Rega and V. Barone, *J. Chem. Phys.*, 2002, **117**, 43–54.
37 (*a*) M. E. Casida, C. Jamorski, K. C. Casida and D. R. Salahub, *J. Chem. Phys.*, 1998, **108**, 4439–4449; (*b*) R. E. Stratmann, G. E. Scuseria and M. J. Frisch, *J. Chem. Phys.*, 1998, **109**, 8218–8224; (*c*) R. Bauernschmitt and R. Ahlrichs, *Chem. Phys. Lett.*, 1996, **256**, 454–464.
38 P. T. Burks, J. V. Garcia, R. GonzalezIrias, J. T. Tillman, M. Niu, A. A. Mikhailovsky, J. Zhang, F. Zhang and P. C. Ford, *J. Am. Chem. Soc.*, 2013, **135**, 18145–18152.
39 (*a*) J. G. Calvert and J. N. Pitts, *Photochemistry*, J. Wiley & Sons, New York, 1967, pp. 783–786; (*b*) G. Malouf and P. C. Ford, *J. Am. Chem. Soc.*, 1977, **99**, 7213–7221.
40 C. F. Works, C. J. Jocher, G. D. Bart, X. Bu and P. C. Ford, *Inorg. Chem.*, 2002, **41**, 3728–3739.

Electronic Supporting Information
for
Syntheses and Properties of Phosphine-Substituted Ruthenium(II) Polypyridine Complexes with Nitrogen Oxides

Go Nakamura,[ab] Mio Kondo,[abcd] Meredith Crisalli,[e] Sze Koon Lee,[a] Akane Shibata,[a] Peter C. Ford,[e] and Shigeyuki Masaoka*[abd]

[a] Institute for Molecular Science (IMS), 5-1 Higashiyama, Myodaiji, Okazaki, Aichi 444-8787, Japan.

[b] Department of Structural Molecular Science, School of Physical Sciences, SOKENDAI (The Graduate University for Advanced Studies), Shonan Village, Hayama-cho, Kanagawa 240-0193, Japan.

[c] ACT-C, Japan Science and Technology Agency (JST), 4-1-8 Honcho, Kawaguchi, Saitama, 332-0012.

[d] Research Center of Integrative Molecular Systems (CIMoS), Institute for Molecular Science 38 Nishigo-naka, Myodaiji, Okazaki, Aichi 444-8585, Japan.

[e] Department of Chemistry and Biochemistry, University of California at Santa Barbara, Santa Barbara, California 93106-9510, United States

E-mail: masaoka@ims.ac.jp

Table of Contents

Reaction of the nitrite complexes with acid

Reactions of *nitrito*-κ*N* complexes with hexafluorophosphoric acid (HPF_6) were studied. Only ***cis*-NO_2** showed large blue shift of MLCT band from 431 nm to 383 nm, suggesting the formation of a corresponding nitrosyl complex. In contrast, ***trans*-NO_2** or **PP-NO_2** reacted with HPF_6 and changed to solvent coordinated complexes (Figures S1-2). This may be due to easy dissociation of the N(O)OH ligand at the *trans* position of the phosphino group in ***trans*-NO_2** or **PP-NO_2**.

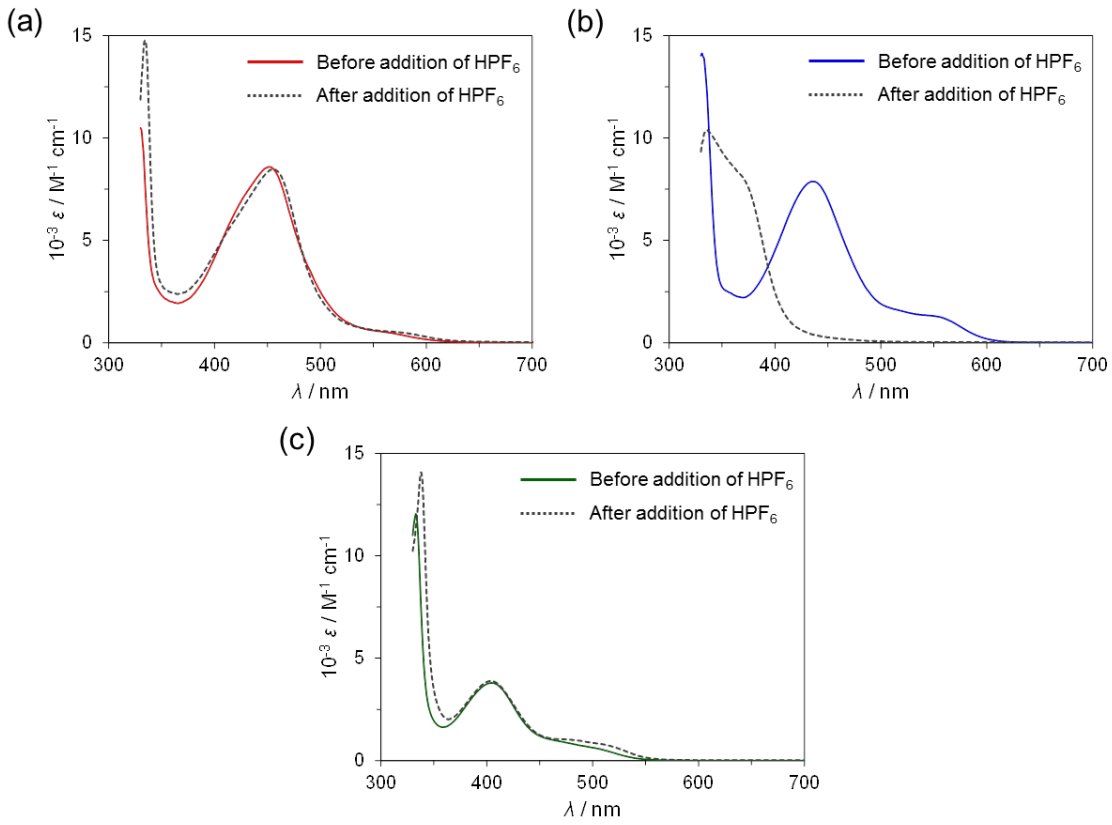

Figure S1 UV-vis absorption spectra of (a) ***trans*-NO_2**, (b) ***cis*-NO_2**, and (c) **PP-NO_2** in acetone at 0 °C before and after the addition of a few drops of HPF_6.

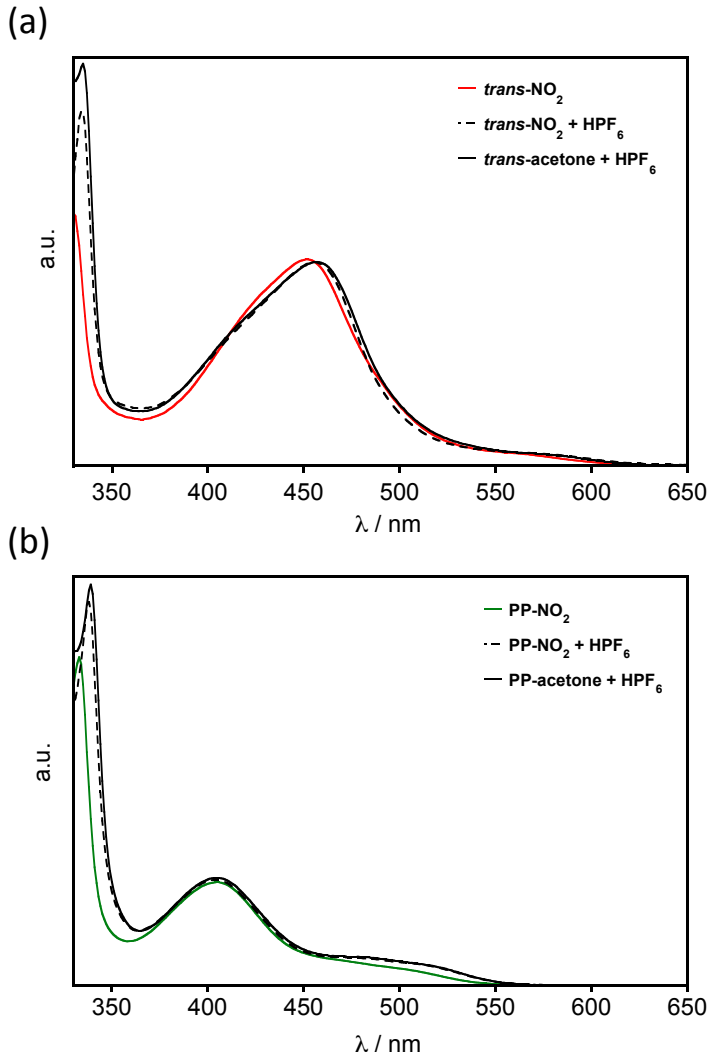

Figure S2 (a) UV-vis absorption spectra of ***trans*-NO_2** before (red solid line) and after (black dashed line) the addition of a few drops of HPF_6 and ***trans*-acetone** in the presence of a few drops of HPF_6 (black solid line) in acetone. (b) UV-vis absorption spectra of **PP-NO_2** before (green solid line) and after (black dashed line) the addition of a few drops of HPF_6 and **PP-acetone** in the presence of a few drops of HPF_6 (black solid line) in acetone. The spectra of *nitrito*-κ*N* complexes after the addition of HPF_6 are almost identical to those of corresponding acetone complexes, which indicates the formation of the solvent coordinated complexes.

Stability of *cis*-NO in Various Solvents

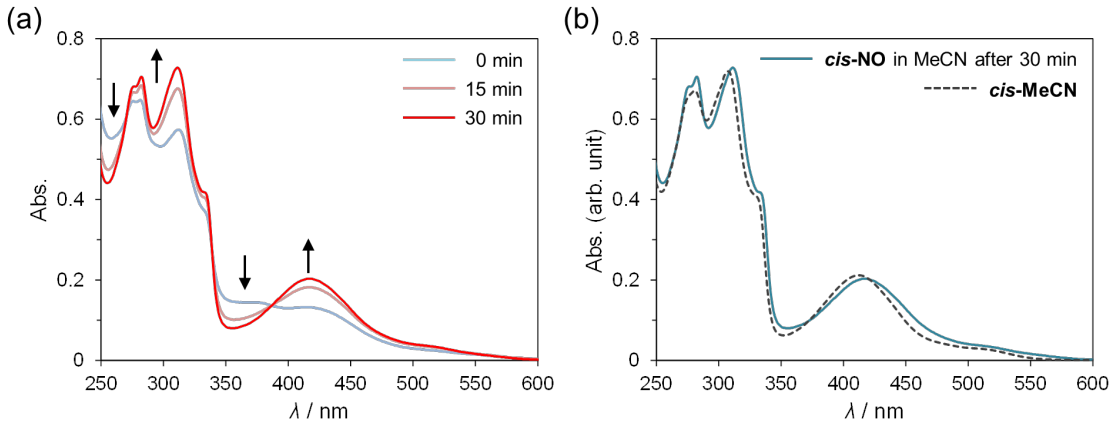

Figure S3 (a) UV-vis absorption spectral changes of ***cis*-NO** in MeCN at room temperature. Dissociation of NO from the complex resulted in the formation of ***cis*-MeCN**. (b) A UV-vis absorption spectrum of ***cis*-NO** in MeCN after 30 min and that of ***cis*-MeCN** in MeCN.

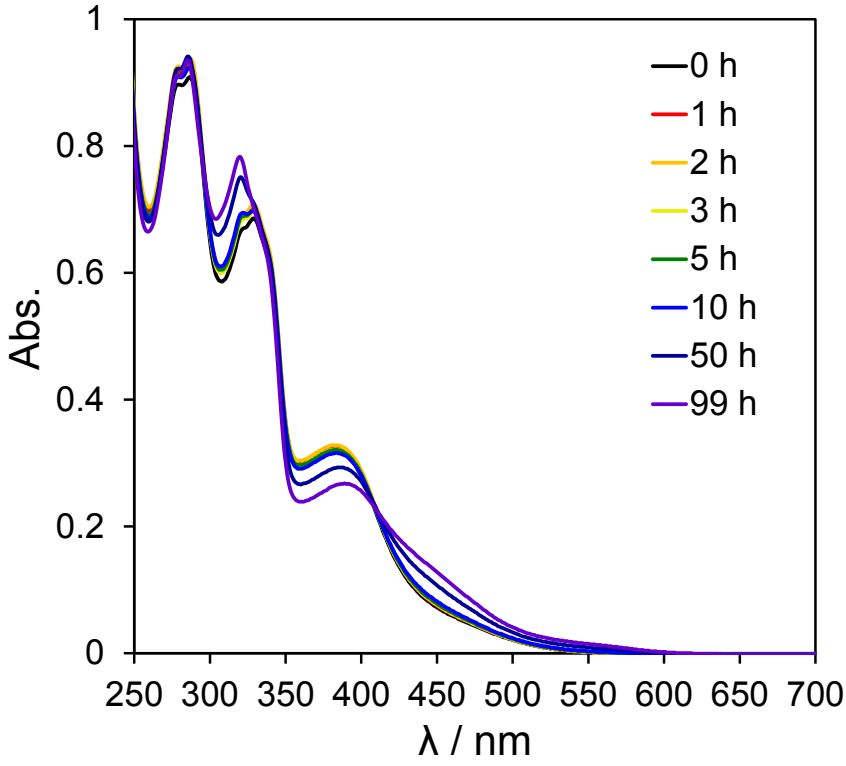

Figure S4 Time course changes of UV-vis absorption spectra of ***cis*-NO** in ethylene glycol at room temperature. ***cis*-NO** exhibited almost no change 3 h after the preparation of the solution, whereas the gradual change was observed after 50 h.

DFT Calculations.

To discuss the electronic structures of ***trans*-NO_2**, ***cis*-NO_2**, and **PP-NO_2**, density functional theory (DFT) calculations were conducted using the Gaussian 09 programs with the B3LYP functional and LanL2DZ basis set. All calculations were performed with the polarizable continuum model (PCM) to account for solvent effects in acetonitrile. All optimized structures were shown in Figure S5.

The highest occupied molecular orbitals (HOMOs, HOMO to HOMO−2) and the lowest unoccupied molecular orbitals (LUMOs, LUMO to LUMO+2) are illustrated in Figure S6. The HOMOs of ***trans*-NO_2** and ***cis*-NO_2** contain dπ (d_{xy}, d_{yz}, and d_{zx}) characteristics of ruthenium with distribution to the π* orbitals of trpy, Pqn, and acetonitrile ligands and σ* orbitals of P−C bonds in the phosphine donors. The LUMOs are dominated mainly by π* orbitals of trpy or Pqn. The frontier orbitals of **PP-NO_2** are similar to those of ***trans*-NO_2** and ***cis*-NO_2**, except that the π* orbitals of dppbz are not involved in orbitals from HOMO−2 to LUMO+2. The HOMO energy levels of ***trans*-NO_2**, ***cis*-NO_2**, and **PP-NO_2** were −6.04, −6.06, and −6.31 eV (Figure S7), respectively, indicating a tendency similar to that observed in the oxidation potentials (E_{pc}) in cyclic voltammograms (0.79, 0.82, and 0.95 V vs Fc/Fc^+).

Electronic transitions for the complexes were investigated using the time-dependent density functional theory (TD-DFT) method. Calculated excitation wavelengths and oscillator strengths for selected transitions are listed in Table S1, and absorption spectra based on these calculated transitions with Gaussian functions are depicted in Figure S8. The profiles of convoluted absorption spectra are similar to those observed experimentally. For ***trans*-NO_2** and ***cis*-NO_2**, transitions in the visible light region arise mainly from the MLCT transition from the dπ orbitals of ruthenium (HOMOs) to the π* orbitals of trpy (LUMO and LUMO+1) and Pqn (LUMO+2). For **PP-NO_2**, the transitions arise mainly from dπ orbitals of ruthenium (HOMOs) to π* orbitals of trpy (LUMO and LUMO+1), which do not involve the π* orbitals of dppbz. Intensity of the simulated absorption of **PP-NO_2** was nearly 50% of those of ***trans*-NO_2** and ***cis*-NO_2**, which is consistent with the experimental results (Figure 3).

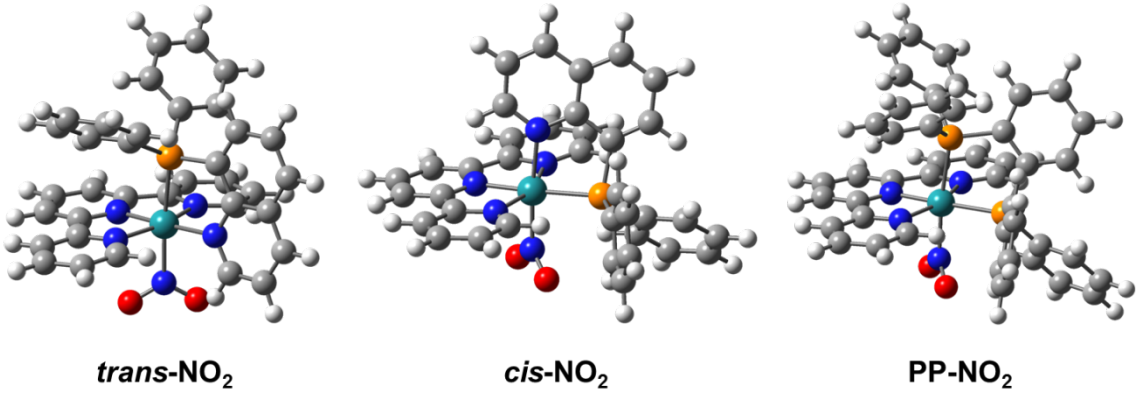

Figure S5 Optimized structures of cationic moieties of ***trans*-NO_2**, ***cis*-NO_2**, and **PP-NO_2**.

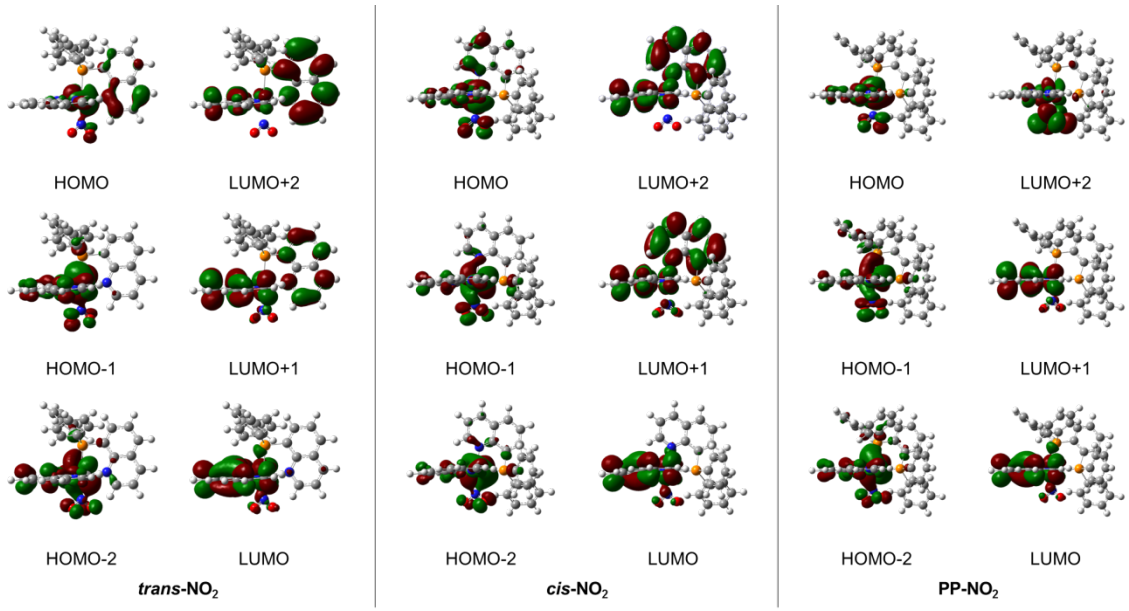

Figure S6 Isodensity surface plots of selected frontier molecular orbitals of ***trans*-NO_2**, ***cis*-NO_2**, and **PP-NO_2** based on the optimized ground-state geometry.

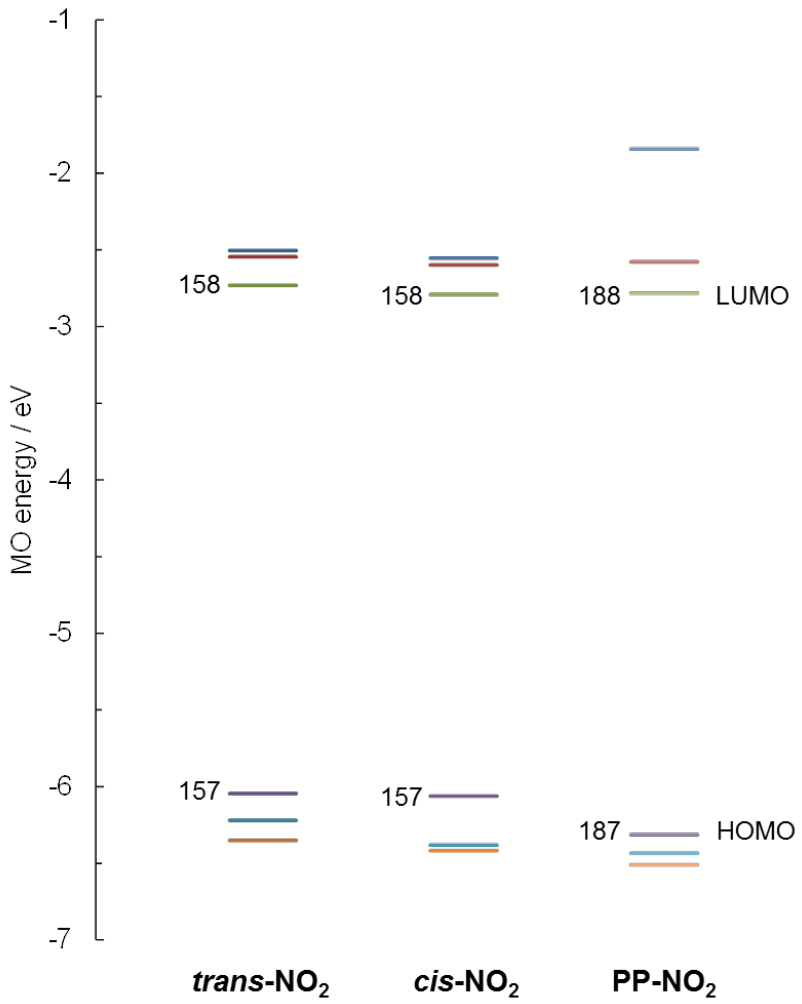

Figure S7 Diagram of DFT-derived molecular orbital energies of ***trans*-NO_2**, ***cis*-NO_2**, and **PP-NO_2**.

Table S1 Calculated TD-DFT excitation energies of ***trans*-NO_2**, ***cis*-NO_2**, and **PP-NO_2** in acetonitrile media. *f* denotes the oscillator strength calculated for each transition.

Complex	λ / nm	*f*	Transition			|CI coef| (> 0.3)
***trans*-NO_2**	440.86	0.0681	HOMO–2	→	LUMO	0.49267
			HOMO	→	LUMO+2	0.37097
	434.46	0.0589	HOMO–1	→	LUMO+1	0.30404
			HOMO	→	LUMO+2	0.49097
	411.01	0.0260	HOMO–2	→	LUMO+1	0.40021
			HOMO–1	→	LUMO+2	0.31482
	404.06	0.0341	HOMO–2	→	LUMO+1	0.53011
***cis*-NO_2**	436.63	0.0714	HOMO	→	LUMO+2	0.49267
	420.79	0.0489	HOMO–2	→	LUMO	0.30590
			HOMO–2	→	LUMO+1	0.34591
			HOMO–1	→	LUMO	0.32855
			HOMO	→	LUMO+1	0.33384
	415.44	0.0200	HOMO–1	→	LUMO+1	0.63146
	407.86	0.0246	HOMO–2	→	LUMO+1	0.58333
PP-NO_2	413.93	0.0299	HOMO–2	→	LUMO+1	0.32625
			HOMO–1	→	LUMO+1	0.35894
			HOMO	→	LUMO+1	0.37271
	402.79	0.0364	HOMO–1	→	LUMO+1	0.59003
	390.03	0.0317	HOMO–2	→	LUMO+1	0.60400

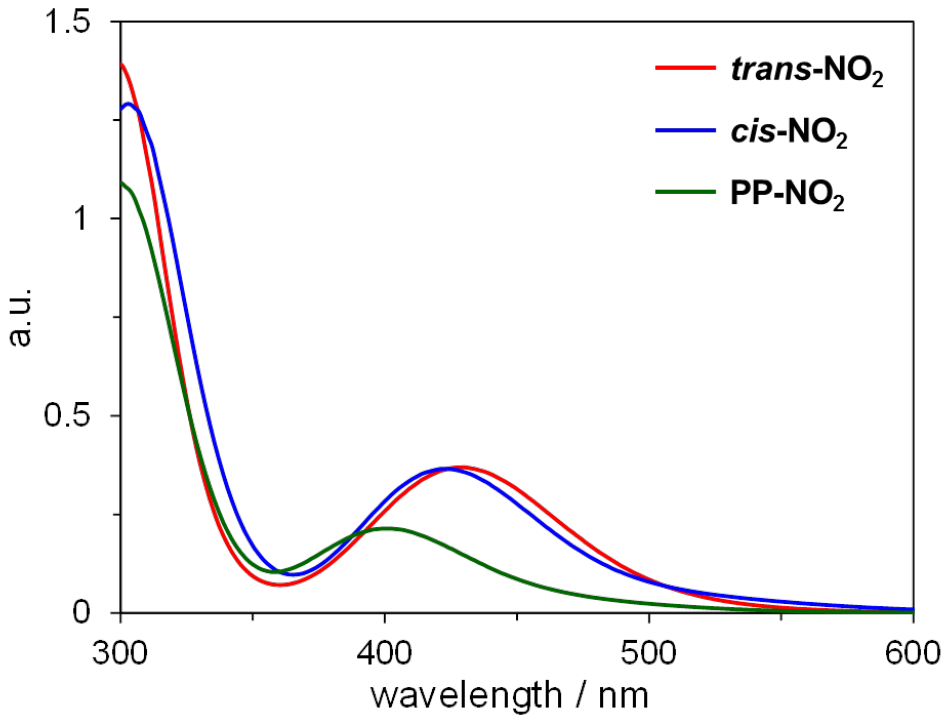

Figure S8 Simulated absorption spectra of ***trans*-NO_2**, ***cis*-NO_2**, and **PP-NO_2** in acetonitrile based on TD-DFT calculations.

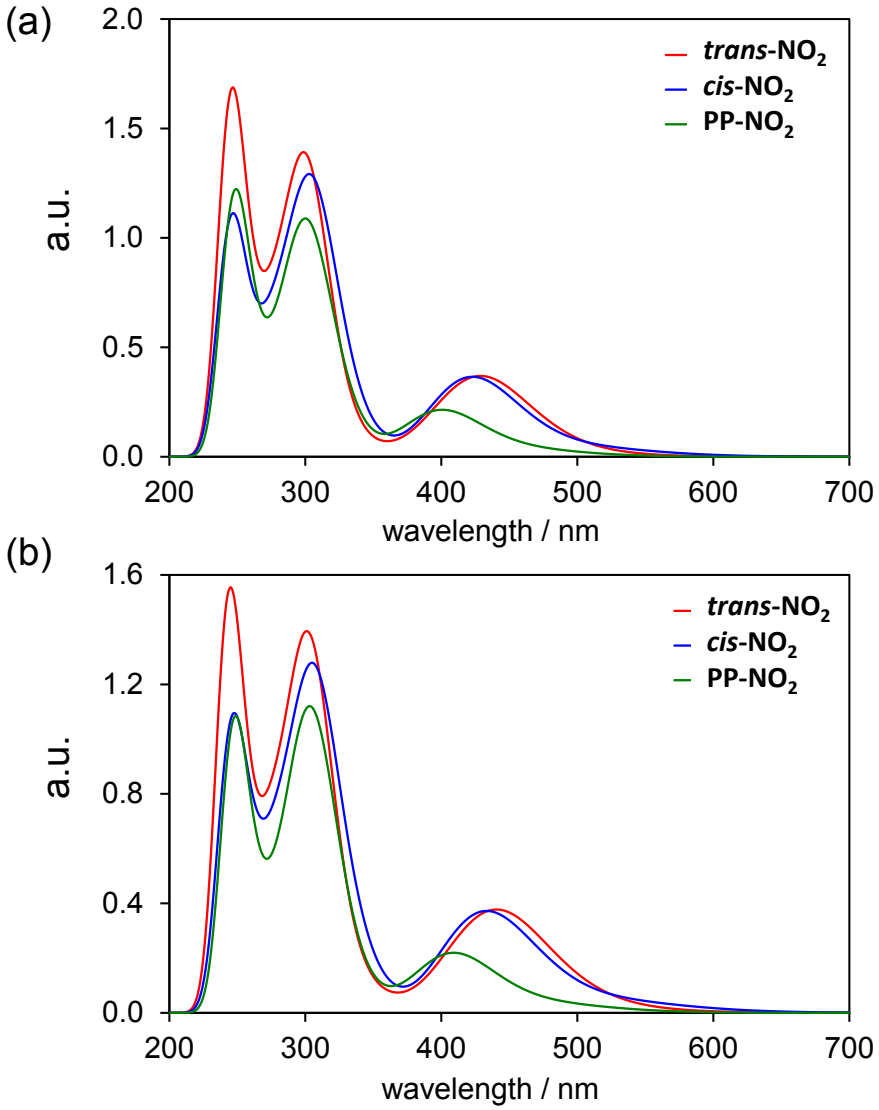

Figure S9 Simulated absorption spectra of ***trans*-NO_2**, ***cis*-NO_2**, and **PP-NO_2** in acetonitrile based on TD-DFT calculations at (a) B3LYP/LanL2DZ and (b) B3LYP/SDD level. The calculation using SDD and LanL2DZ afford the almost same results for all complexes.

Cyclic Voltammograms

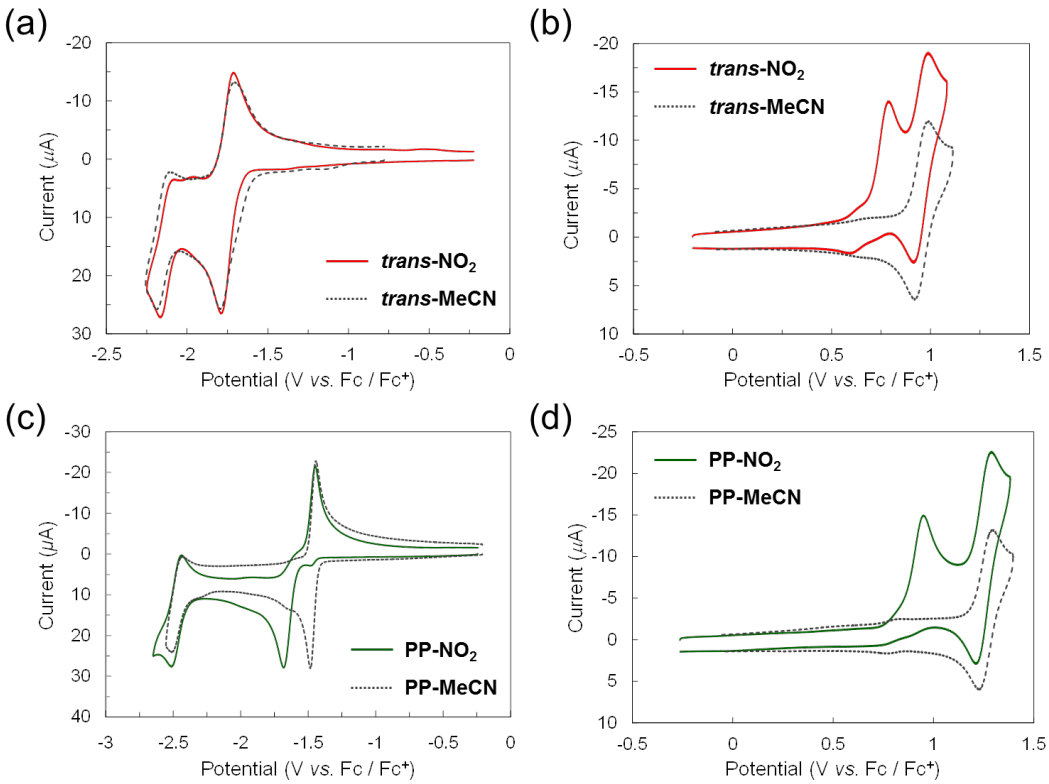

Figure S10 (a), (b) Cyclic voltammograms of ***trans*-NO$_2$** and ***trans*-MeCN** (0.5 mM) in 0.1 M TEAP/acetonitrile under an Ar atmosphere. (c), (d) Cyclic voltammograms of **PP-NO$_2$** and **PP-MeCN** (0.5 mM) in 0.1 M TEAP/acetonitrile under an Ar atmosphere (WE: GC, CE: Pt wire, RE: Ag/Ag$^+$; Scan rate: 100 mV/s).

Photostability of *cis*-NO

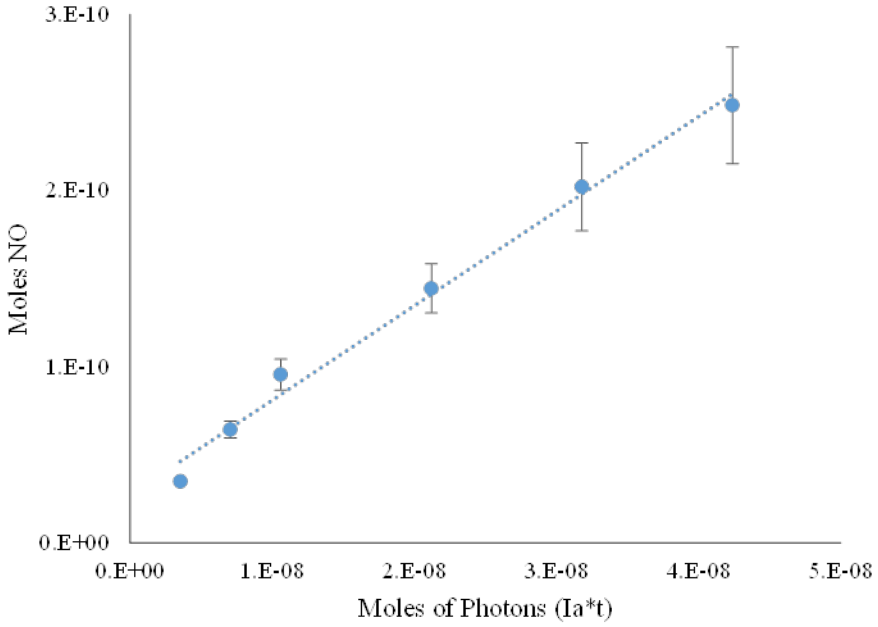

Figure S11 Plots of moles of NO vs photons for the photorelease of ***cis*-NO** when irradiated at 365 nm under air conditions. Error bars reflect one standard deviation of the cumulative moles of NO produced over the duration of the experiment. The slope is equal to quantum yield. From these data, a quantum yield of 0.0048 under air conditions was calculated.

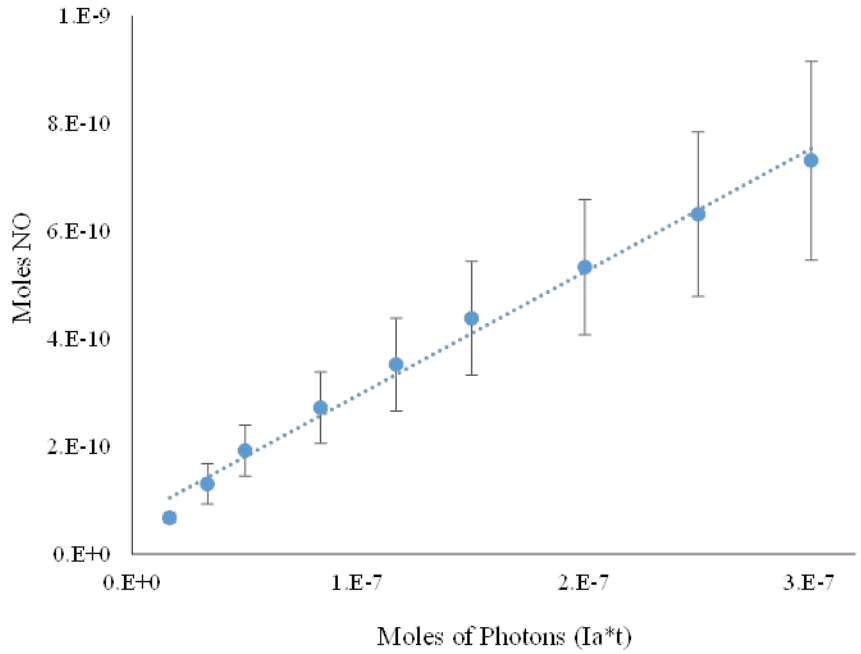

Figure S12 Plots of moles of NO vs photons for the photorelease of ***cis*-NO** when irradiated at 365 nm under helium. Error bars reflect one standard deviation of the cumulative moles of NO produced over the duration of the experiment. The slope is equal to quantum yield. From these data, a quantum yield of 0.0025 under helium was calculated.

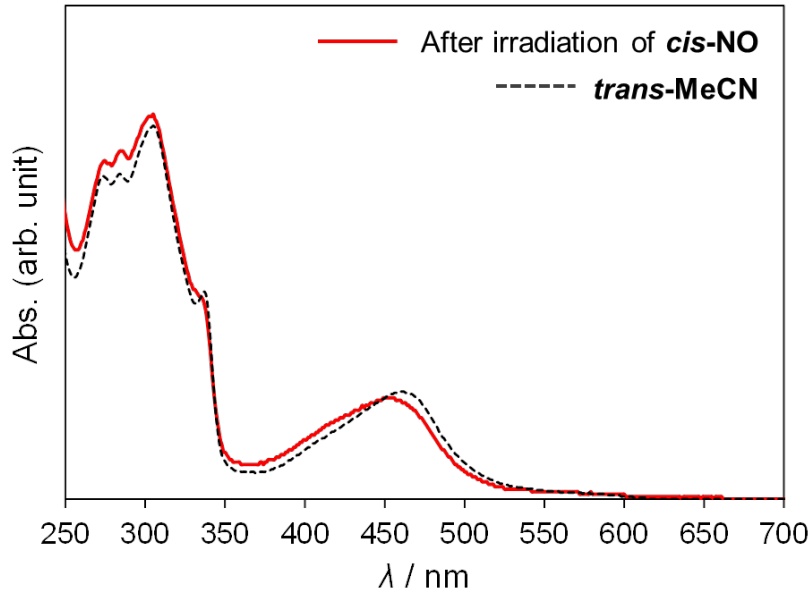

Figure S13. A UV-vis absorption spectrum of ***cis*-NO** in ethylene glycol after photoirradiation of 355 nm laser for 2048 times (pulse width = 5 ns, beam diameter incident on the sample = 6 mm, repetition rate = 5 Hz) and that of ***trans*-MeCN** in ethylene glycol at room temperature.

Stability of MeCN complexes

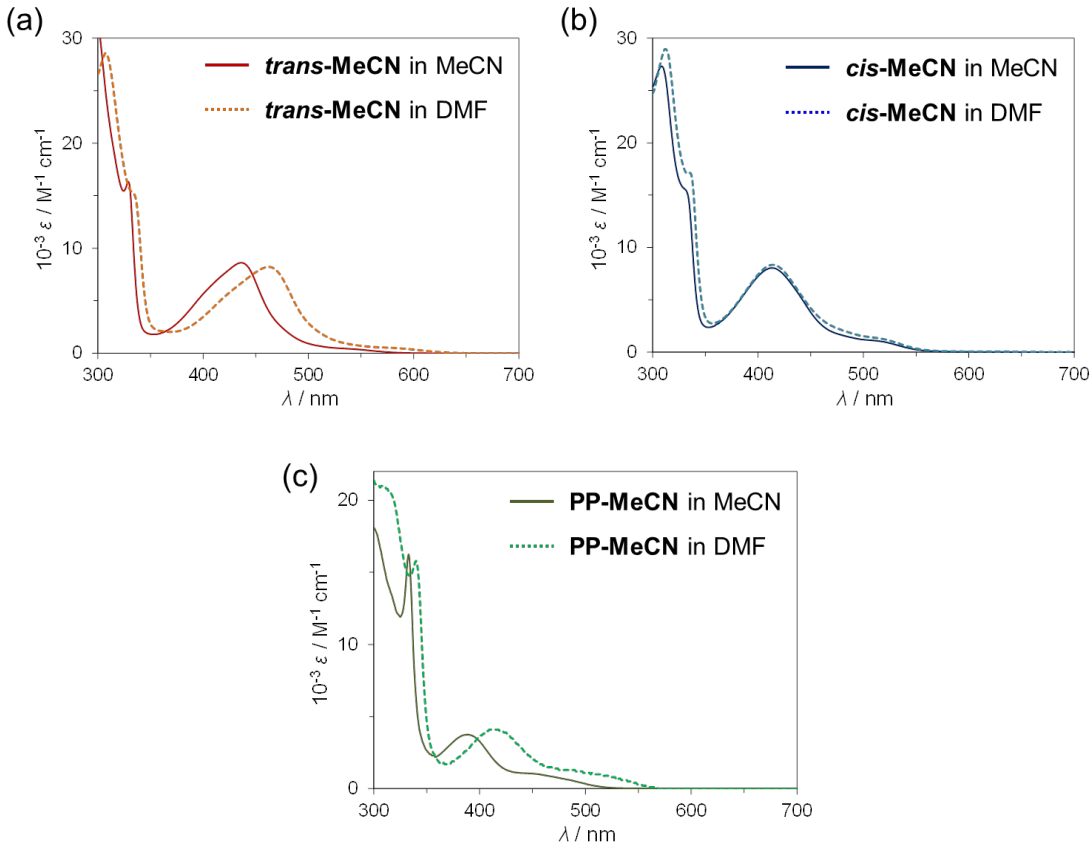

Figure S14 UV-vis absorption spectra of ***trans*-MeCN**, ***cis*-MeCN** and **PP-MeCN** in acetonitrile and DMF at room temperature. The UV-vis spectra indicate that the acetonitrile ligand of ***trans*-MeCN** and **PP-MeCN** can easily undergo a ligand substitution and form *trans(P,DMF)*-[Ru(trpy)(Pqn)(DMF)]$(PF_6)_2$ (***trans*-DMF**) and [Ru(trpy)(dppbz)(DMF)]$(PF_6)_2$ (**PP-DMF**), whereas that of ***cis*-MeCN** is barely substituted.

Single Crystal X-ray Structure Determination

Table S2 Selected bond distances (Å) and angles (°) for ***trans*-NO_2**, ***cis*-NO_2'**, and **PP-NO_2**

***trans*-NO_2**·CH_3CN		***cis*-NO_2'**·0.5CH_3CN				**PP-NO_2**·2CH_3OH	
Ru1–N1	2.085(4)	Ru1–N1	2.1066(18)	Ru2–N6	2.1353(19)	Ru1–N1	2.125(2)
Ru1–N2	1.971(4)	Ru1–N2	2.0153(18)	Ru2–N7	2.0248(19)	Ru1–N2	2.020(2)
Ru1–N3	2.081(4)	Ru1–N3	2.1066(18)	Ru2–N8	2.1012(19)	Ru1–N3	2.095(2)
Ru1–N4	2.143(4)	Ru1–N4	2.1080(18)	Ru2–N9	2.1241(18)	Ru1–N4	2.124(2)
Ru1–N5	2.146(4)	Ru1–N5	2.0362(18)	Ru2–N10	2.0290(18)	Ru1–P1	2.2958(7)
Ru1–P1	2.2952(13)	Ru1–P1	2.2981(6)	Ru2–P2	2.3005(6)	Ru1–P2	2.3270(7)
N5–O1	1.199(6)	N5–O1	1.251(3)	N10–O3	1.253(3)	N4–O1	1.252(3)
N5–O2	1.246(6)	N5–O2	1.251(3)	N10–O4	1.253(3)	N4–O2	1.229(3)
N1–Ru1–N2	79.00(17)	N1–Ru1–N2	78.31(7)	N6–Ru2–N7	77.74(8)	N1–Ru1–N2	77.59(9)
N2–Ru1–N3	79.43(17)	N2–Ru1–N3	78.35(8)	N7–Ru2–N8	78.25(7)	N2–Ru1–N3	78.46(9)
N4–Ru1–P1	82.00(12)	N4–Ru1–P1	82.65(5)	N9–Ru2–P2	82.51(5)	P1–Ru1–P2	84.10(3)
O1–N5–O2	122.4(5)	O1–N5–O2	117.75(19)	O3–N10–O4	118.00(18)	O1–N4–O2	118.5(2)